SIAM J. IMAGING SCIENCES
Vol. 7, No. 2, pp. 867–899

Near-Field Imaging of Infinite Rough Surfaces in Dielectric Media*

Gang Bao† and Peijun Li‡

Abstract. This paper is concerned with an inverse surface scattering problem in near-field optical imaging, which is to reconstruct the scattering surface of a dielectric medium with a resolution beyond the diffraction limit. It is a nontrivial extension of the authors' work on near-field imaging of infinite rough surfaces from impenetrable to penetrable media [G. Bao and P. Li, *SIAM J. Appl. Math.*, 73 (2013), pp. 2162–2187], where a more sophisticated transmission problem needs to be considered. The scattering surface is modeled as a small and smooth deformation of a plan surface. Based on a transformed field expansion, an analytic solution, which is given as a power series, is derived for the direct scattering problem. By neglecting high order terms in the power series, the original nonlinear inverse problem is linearized; explicit and unified reconstruction formulas are deduced for both reflection and transmission configurations. A spectral cut-off regularization is adopted to suppress the exponential growth of the noise in the evanescent wave components, which carry high spatial frequency of the scattering surface and contribute to the superresolution in the near-field regime. The method requires only a single illumination at a fixed frequency and is realized efficiently by the fast Fourier transform. Numerical results show that the method is simple, stable, and effective in reconstructing scattering surfaces of dielectric media with subwavelength resolution.

Key words. inverse surface scattering, transformed field expansion, near-field imaging, Helmholtz equation

AMS subject classifications. 65N21, 78A46

DOI. 10.1137/130944485

1. Introduction.

Scattering problems are concerned with how an inhomogeneous medium scatters an incident field. Given the incident field, the direct scattering problem is to determine the scattered field, while the inverse scattering problem is to determine the nature of the inhomogeneity, such as geometry and material property, from the measured scattered field [21]. These problems have played a fundamental role in diverse scientific areas such as radar and sonar, geophysical exploration, and medical imaging. However, there is a resolution limit to the sharpness of details that can be observed by conventional far-field optical microscopy, one-half the wavelength, referred to as the Rayleigh criterion or the diffraction limit [23]. Near-field optical imaging is an effective approach to breaking the diffraction limit and obtaining images with subwavelength resolution [22], which leads to exciting applications in broad areas of modern science and technology, including surface chemistry, biology, materials science, and information storage. This paper is a nontrivial extension of the authors' work in [9] on near-

*Received by the editors November 7, 2013; accepted for publication (in revised form) January 29, 2014; published electronically May 1, 2014.
http://www.siam.org/journals/siims/7-2/94448.html

†Department of Mathematics, Zhejiang University, Hangzhou 310027, China, and Department of Mathematics, Michigan State University, East Lansing, MI 48824 (drbaogang@gmail.com). This author's research was supported in part by NSF grants DMS-0968360 and DMS-1211292, ONR grant N00014-12-1-0319, a Key Project of the Major Research Plan of NSFC (91130004), and a special research grant from Zhejiang University.

‡Department of Mathematics, Purdue University, West Lafayette, IN 47907 (lipeijun@math.purdue.edu). This author's research was supported in part by NSF grant DMS-1151308.

field imaging of infinite rough surfaces from impenetrable media to penetrable dielectric media since a more complicated transmission problem needs to be considered. It aims to develop an effective mathematical model and design an efficient computational method for solving the inverse scattering problem that arises in near-field optical imaging of infinite rough surfaces in dielectric media.

We study a model problem of the scattering by an infinite rough surface, which is usually referred to as a nonlocal perturbation of an infinite plane surface such that the whole surface lies within a finite distance of the original plane. The wave motion is governed by the two-dimensional Helmholtz equation, which describes the propagation of acoustic waves or the transverse electric polarization of electromagnetic waves. Specifically, we consider the scattering of a time-harmonic plane wave incident on a penetrable rough surface from the top, where the spaces above and below the scattering surface are filled with some homogeneous medium, respectively. In the applications of near-field imaging, it is reasonable to assume that the scattering surface is a small and smooth deformation of a plane surface. The deformation is allowed to be very general. Examples include a nonlocal perturbation of a plane surface, which is referred to as an unbounded rough surface [40, 41]; a local perturbation of a plane surface, which is called a cavity wall [29]; a periodic structure, which is known as a grating surface [2, 6]. Given the scattering surface and a time-harmonic plane incident wave, the direct scattering problem is to predict the wave field distribution away from the surface. We are mainly interested in studying the inverse scattering problem: what information can we extract about the surface from the wave field measured at a constant distance above the scattering surface, which is called the reflection configuration, or below the scattering surface, which is called the transmission configuration, particularly in the near-field regime, i.e., at a distance which is much smaller than the wavelength of the incident wave?

The direct problem has been examined extensively by numerous researchers via either integral equation methods or variational approaches in the aforementioned three modalities, such as the unbounded rough surface scattering [16, 25, 33, 37, 42, 43], the cavity scattering problem [3, 8, 32], the diffraction grating problem [7], and references cited therein. The inverse problem has also been investigated widely for these modalities; see [1, 10, 11, 20, 26, 30, 32] and references therein. These results addressed conventional far-field imaging, where the role of evanescent wave components was ignored and the resolution of reconstructions was restricted by the Rayleigh criterion or the diffraction limit. As shown experimentally [28], a light beam illuminating on a sample characterized by a fine structure may be converted into propagating components, which are able to propagate towards the remote detector, and evanescent components, which are confined on the surface. The former are associated to the low spatial frequencies of the sample, whereas the later are connected to their high frequencies, which do not obey the Rayleigh criterion and contribute to the subwavelength resolution. However, it is severely ill-posed to directly make use of the evanescent waves since the noise in the measurements is amplified exponentially and all the useful information is covered by it. Thus, it is important to consider a regularization technique to suppress the exponential growth of the noise in the evanescent wave components. A trade-off is necessary between the resolution and the signal-to-noise ratio (SNR) of the data in order to obtain a stable and superresolved reconstruction. We refer the reader to [4, 5] for the resolution and stability analysis of a related wave imaging problem.

In this paper, we consider a rigorous mathematical model for a class of surface scattering problems in near-field optical imaging. The model problem is formulated as a boundary value problem for the two-dimensional Helmholtz equation with transparent boundary conditions proposed on plane surfaces confining the scattering surface. Based on a transformed field expansion, the boundary value problem with complex scattering surface is reduced into a successive sequence of the Helmholtz equation with plane surfaces. The reduced problem is further converted into a two-point boundary value problem in the frequency domain and is solved analytically by the method of integration solution. For the transformed field expansion method and related boundary perturbation method, we refer the reader to [13, 31, 35, 38, 39] for solving the direct diffraction grating problem and the direct unbounded rough surface scattering problem, respectively. A boundary perturbation method may be found in [36] for solving an inverse scattering problem with a periodic surface. By neglecting the high order terms in the power series for the analytical solution, the nonlinear inverse problem is linearized, and explicit and unified inversion formulas are deduced for both reflection and transmission configurations. The inversion method requires only a single illumination of a plane wave, particularly the normal incidence, at a fixed frequency, and can be done efficiently by the fast Fourier transform (FFT). Spectral cut-off regularization is adopted to suppress the exponential growth of the evanescent wave modes. Results show that the method is simple, stable, and effective in reconstructing scattering surfaces with superresolved resolution.

We point out two closely related papers on the inverse surface scattering in near-field imaging [12, 24], where the scattering surface is assumed to be a perfect electric conductor and a local perturbation of a plane surface and thus the usual Sommerfeld radiation condition is imposed for the scattered field in their model problem. We consider a general scattering surface, and the Sommerfeld radiation condition may no longer be valid for the case of a nonlocal perturbation of a plane surface, such as for the unbounded rough surface scattering problem and the diffraction grating problem. An appropriate transparent boundary condition needs to be imposed for our model problem. In addition, we give a more rigorous argument for the linearization procedure and the dependence of the resolution on the parameters of the deformation parameter, measurement distance, and noise level. Other related work may be found in [14, 15] for solving an inverse medium scattering problem in near-field optical imaging.

The outline of this paper is as follows. In section 2, a mathematical model is introduced and formulated into a boundary value problem by using transparent boundary conditions. A transformed field expansion is presented to analytically derive the solution for the direct surface scattering problem in section 3. Section 4 is devoted to the derivation of explicit inversion formulas of the inverse surface scattering problem for both reflection and transmission configurations. In section 5, numerical implementations are discussed and numerical examples are reported to demonstrate the effectiveness of the proposed method. The paper is concluded with some general remarks and directions for future research in section 6.

2. Model problem.

In this section, we introduce a mathematical model, define some notation for the scattering by a penetrable dielectric rough surface, and present a boundary value problem for the rough surface scattering model.

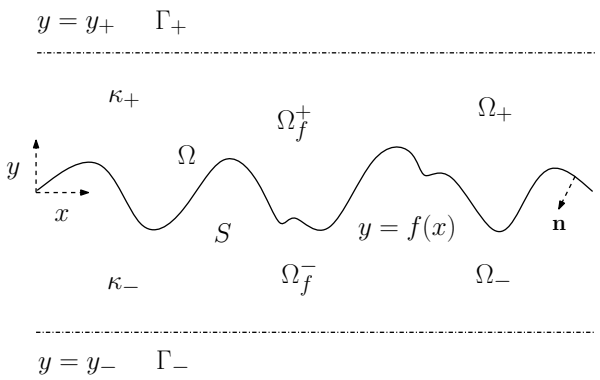

Figure 1. *Problem geometry. A plane wave is incident on the scattering surface S from the top. The spaces Ω_f^+ (above S) and Ω_f^- (below S) are filled with homogeneous materials which are characterized by two different constant wavenumbers κ_+ and κ_-, respectively.*

2.1. Helmholtz equation. As seen in Figure 1, we let the scattering surface be described by the curve $S = \{(x, y) \in \mathbb{R}^2 : y = f(x),\ x \in \mathbb{R}\}$. Here the function f takes the form

$$f(x) = \varepsilon g(x), \quad g \in C^2(\mathbb{R}), \tag{2.1}$$

where ε is a sufficiently small positive constant and is called the surface deformation parameter. Using the scattering surface model (2.1), we assume that the scattering surface is a small and smooth deformation of a plane surface $\Gamma = \{(x, y) \in \mathbb{R}^2 : y = 0\}$.

The scattering surface S is embedded in the rectangular slab

$$\Omega = \{(x, y) \in \mathbb{R}^2 : y_- < y < y_+\} = \mathbb{R} \times (y_-, y_+),$$

where $y_+ > 0$ and $y_- < 0$ are two constants. Hence the domain Ω is bounded above by the plane surface $\Gamma_+ = \{(x, y) \in \mathbb{R}^2 : y = y_+\}$ and bounded blow by the plane surface $\Gamma_- = \{(x, y) \in \mathbb{R}^2 : y = y_-\}$. Two important roles define the artificial boundary surfaces $\Gamma_\pm$: one is that transparent boundary conditions will be imposed on $\Gamma_\pm$; the other is that the scattering data will be measured on $\Gamma_\pm$.

Let $\Omega_f^+ = \{(x, y) \in \mathbb{R}^2 : y > f(x)\}$ and $\Omega_f^- = \{(x, y) \in \mathbb{R}^2 : y < f(x)\}$ be filled with homogeneous materials which are characterized by two different constant wavenumbers κ_+ and κ_-, respectively. In fact, the wavenumbers satisfy $\kappa_\pm^2 = \omega^2 \mu \varepsilon_\pm$, where ω is the angular frequency, μ is the magnetic permeability, which is assumed to be a constant everywhere, and $\varepsilon_\pm$ are the electric permittivity in $\Omega_f^\pm$. In this work, ε_+ is assumed to be a positive constant, i.e., $\varepsilon_+ > 0$, and ε_- is assumed to satisfy $\operatorname{Re} \varepsilon_- > 0, \operatorname{Im} \varepsilon_- \geq 0$. Thus, the medium is allowed to be lossy in Ω_f^- for energy absorption.

Let an incoming plane wave

$$u^{\text{inc}}(x, y) = e^{\mathrm{i}(\alpha x - \beta_+ y)} \tag{2.2}$$

be incident on the scattering surface S from above, where

$$\alpha = \kappa_+ \sin\theta, \quad \beta_+ = \kappa_+ \cos\theta,$$

and $\theta \in (-\pi/2, \pi/2)$ is the angle of incidence with respect to the positive y-axis. The associated wavelength of the incident wave is $\lambda = 2\pi/\kappa_+$. For normal incidence, i.e., $\theta = 0$, we have $\alpha = 0, \beta_+ = \kappa_+$ and the incident field reduces to $u^{\text{inc}}(x, y) = e^{-\text{i}\kappa_+ y}$. As mentioned in the introduction, the proposed method requires only a single illumination of the plane wave at a fixed frequency. We will particularly focus on the case of normal incidence when deriving reconstruction formulas to determine the scattering surface. It can be verified that the incident wave satisfies

$$\Delta u^{\text{inc}} + \kappa_+^2 u^{\text{inc}} = 0 \quad \text{in } \Omega_f^+. \tag{2.3}$$

The scattering of time-harmonic electromagnetic waves in the transverse electric polarization can be modeled by the two-dimensional Helmholtz equation:

$$\Delta u + \kappa^2 u = 0 \quad \text{in } \mathbb{R}^2, \tag{2.4}$$

where u is the total field and the wavenumber

$$\kappa = \begin{cases} \kappa_+ & \text{in} \quad \Omega_f^+, \\ \kappa_- & \text{in} \quad \Omega_f^-. \end{cases} \tag{2.5}$$

Due to the interaction between the incident field and the scattering surface, the total field u can be decomposed into

$$u = \begin{cases} u^{\text{inc}} + u^{\text{s}} & \text{in} \quad \Omega_f^+, \\ u^{\text{s}} & \text{in} \quad \Omega_f^-, \end{cases} \tag{2.6}$$

where u^{s} is the scattered field. For the infinite surface scattering problem, the usual Sommerfeld radiation condition may not be valid for the scattered field. We impose the following bounded outgoing wave condition: the scattered field u^{s} consists of bounded outgoing waves. We refer the reader to [17, 18] for studies of the unbounded rough surface scattering problem with a Dirichlet or an impedance boundary condition by introducing an upward propagating radiation condition.

There are two problems to be solved, the direct surface scattering problem and the inverse surface scattering problem. The direct problem is to determine the total field u, given the incident field u^{inc} and the scattering surface function f. This paper is focused on the inverse surface scattering problem, which is to reconstruct the scattering surface function f from the measurement of the total field u, given the incident field u^{inc}. More specifically, this work is to reconstruct the function $f(x)$ from noisy data of the total field measured either at Γ_+, which is called the reflection configuration, or at Γ_-, which is called the transmission configuration, corresponding to a fixed wavenumber and a single incident direction. In particular, we are interested in the inverse scattering in a near-field regime where the measurement distance $|y_\pm|$ is much smaller than the wavelength λ, i.e., $|y_\pm| \ll \lambda$.

2.2. Transparent boundary condition. We introduce transparent boundary conditions on $\Gamma_\pm$, which are equivalent to the bounded outgoing wave condition. Since the derivations of the transparent boundary conditions on Γ_+ and Γ_- are analogous, we derive only the transparent

boundary condition on Γ_+ and state the corresponding transparent boundary condition on Γ_-.

Given a function $u(x)$, the one-dimensional Fourier transform of u is defined by

$$\hat{u}(\xi) = (2\pi)^{-1/2} \int_{\mathbb{R}} u(x) e^{-\mathrm{i}x\xi} dx.$$

It follows from (2.3), (2.4), and (2.6) that the scattered field satisfies

$$\Delta u^{\mathrm{s}} + \kappa_+^2 u^{\mathrm{s}} = 0 \quad \text{for } y > y_+. \tag{2.7}$$

Taking the Fourier transform of (2.7) with respect to x, we have

$$\frac{\partial^2 \hat{u}^{\mathrm{s}}(\xi, y)}{\partial y^2} + (\kappa_+^2 - \xi^2)\hat{u}^{\mathrm{s}}(\xi, y) = 0 \quad \text{for } y > y_+. \tag{2.8}$$

Noting the outgoing wave condition for the scattered field, the solution of (2.8) may be given by

$$\hat{u}^{\mathrm{s}}(\xi, y) = \hat{u}^{\mathrm{s}}(\xi, y_+) e^{\mathrm{i}\eta_+(y-y_+)}, \tag{2.9}$$

where

$$\eta_+^2(\xi) = \kappa_+^2 - \xi^2 \quad \text{with } \mathrm{Im}\eta_+(\xi) \geq 0. \tag{2.10}$$

Taking the inverse Fourier transform on both sides of (2.9), we obtain

$$u^{\mathrm{s}}(x, y) = (2\pi)^{-1/2} \int_{\mathbb{R}} \hat{u}^{\mathrm{s}}(\xi, y_+) e^{\mathrm{i}\eta_+(y-y_+)} e^{\mathrm{i}\xi x} d\xi.$$

Taking the partial derivative with respect to y and then evaluating at $y = y_+$ on both sides of the above equation yield

$$\partial_y u^{\mathrm{s}}(x, y_+) = (2\pi)^{-1/2} \int_{\mathbb{R}} \mathrm{i}\eta_+ \hat{u}^{\mathrm{s}}(\xi, y_+) e^{\mathrm{i}\xi x} d\xi.$$

For any given u on Γ_+, i.e., $u(x, y_+)$, we define a boundary operator T_+:

$$T_+ u = (2\pi)^{-1/2} \int_{\mathbb{R}} \mathrm{i}\eta_+(\xi) \hat{u}(\xi, y_+) e^{\mathrm{i}\xi x} d\xi,$$

which maps $u(x, y_+)$ to $\partial_y u(x, y_+)$. Noticing the field decomposition in Ω_+ from (2.6), we deduce a transparent boundary condition on Γ_+:

$$\partial_y (u - u^{\mathrm{inc}}) = T_+ (u - u^{\mathrm{inc}}).$$

Equivalently, it can be reformulated in terms of the total field:

$$\partial_y u - T_+ u = \phi_+ \quad \text{on } \Gamma_+, \tag{2.11}$$

where

$$\phi_+ = \partial_y u^{\text{inc}} - T_+ u^{\text{inc}} = -2\mathrm{i}\beta e^{\mathrm{i}(\alpha x - \beta y_+)}. \tag{2.12}$$

Similarly, for any given u on Γ_-, i.e., $u(x, y_-)$, we define a boundary operator T_-:

$$T_- u = (2\pi)^{-1/2} \int_{\mathbb{R}^2} \mathrm{i}\eta_-(\xi)\hat{u}(\xi, y_-)e^{\mathrm{i}\xi x} d\xi,$$

where

$$\eta_-^2(\xi) = \kappa_-^2 - \xi^2 \quad \text{with } \mathrm{Im}\eta_-(\xi) \geq 0. \tag{2.13}$$

A transparent boundary condition on Γ_- can be written as

$$\partial_y u + T_- u = \phi_- \quad \text{on } \Gamma_-, \tag{2.14}$$

where

$$\phi_- = 0. \tag{2.15}$$

Clearly, the transparent boundary conditions (2.11) and (2.14) are nonlocal in the physical domain. However, they are local boundary conditions in the frequency domain, which makes it possible to derive an analytical solution for the direct problem in section 3.

2.3. Transmission problem. We reformulate the boundary value problem (2.4), (2.11), (2.14) into an equivalent transmission problem, which has a more convenient form for introducing the method of transformed field expansion.

Denote $\Omega_+ = \Omega_f^+ \cap \Omega = \{(x, y) \in \mathbb{R}^2 : f(x) < y < y_+\}$ and $\Omega_- = \Omega_f^- \cap \Omega = \{(x, y) \in \mathbb{R}^2 : y_- < y < f(x)\}$, as seen in Figure 1. Let $u^+ = u|_{\Omega_+}$ and $u^- = u|_{\Omega_-}$; then it follows from (2.4) and (2.5) that we have

$$\Delta u^\pm + \kappa_\pm^2 u^\pm = 0 \quad \text{in } \Omega_\pm. \tag{2.16}$$

Recall the nonlocal transparent boundary conditions (2.11) and (2.14):

$$\partial_y u^\pm \mp T_\pm u^\pm = \phi^\pm \quad \text{on } \Gamma_\pm. \tag{2.17}$$

Following from the jump conditions, we obtain that the field and its normal derivatives are continuous across the scattering surface S; i.e.,

$$u^+(x, f(x)) = u^-(x, f(x)) \quad \text{and} \quad \partial_{\mathbf{n}} u^+(x, f(x)) = \partial_{\mathbf{n}} u^-(x, f(x)), \tag{2.18}$$

where $\mathbf{n} = (n_1, n_2)$ is the unit normal vector on S pointing from Ω_+ to Ω_-. Explicitly, we have

$$n_1 = \frac{f'(x)}{(1 + (f'(x))^2)^{1/2}} \quad \text{and} \quad n_2 = \frac{-1}{(1 + (f'(x))^2)^{1/2}}.$$

Hence the transmission problem is to find the fields u^+ and u^- in Ω^+ and Ω^-, respectively, such that they satisfy the Helmholtz equations (2.16), the boundary conditions (2.17), and the continuity conditions (2.18).

3. Transformed field expansion. In this section, we introduce the transformed field expansion to analytically derive the solution for the transmission problem (2.16)–(2.18). The solution is given as a power series of the surface deformation parameter ε and plays an important role for our reconstruction formulas.

3.1. Change of variables. The transformed field expansion method, as applied to the surface scattering, begins with the change of variables

$$\tilde{x} = x, \quad \tilde{y} = y_+ \left(\frac{y - f}{y_+ - f} \right), \quad f < y < y_+,$$

and

$$\tilde{x} = x, \quad \tilde{y} = y_- \left(\frac{y - f}{y_- - f} \right), \quad y_- < y < f,$$

which maps Ω_+ and Ω_- into rectangular slabs $D_+ = \{(\tilde{x}, \tilde{y}) \in \mathbb{R}^2 : 0 < \tilde{y} < y_+\}$ and $D_- = \{(\tilde{x}, \tilde{y}) \in \mathbb{R}^2 : y_- < \tilde{y} < 0\}$, respectively.

We now seek to restate the transmission problem (2.16)–(2.18) in the transformed coordinates. It is easy to verify the differentiation rules

$$\partial_x = \partial_{\tilde{x}} - f' \left(\frac{y_+ - \tilde{y}}{y_+ - f} \right) \partial_{\tilde{y}}, \quad \partial_y = \left(\frac{y_+}{y_+ - f} \right) \partial_{\tilde{y}} \quad \text{for } f < y < y_+$$

and

$$\partial_x = \partial_{\tilde{x}} - f' \left(\frac{y_- - \tilde{y}}{y_- - f} \right) \partial_{\tilde{y}}, \quad \partial_y = \left(\frac{y_-}{y_- - f} \right) \partial_{\tilde{y}} \quad \text{for } y_- < y < f.$$

Introduce new functions $w^{\pm}(\tilde{x}, \tilde{y}) = u^{\pm}(x, y)$ under the transformation. It can be verified after tedious but straightforward calculations that $w^{\pm}$, upon dropping the prime, satisfy the equation

$$c_1^{\pm} \frac{\partial^2 w^{\pm}}{\partial x^2} + c_2^{\pm} \frac{\partial^2 w^{\pm}}{\partial y^2} - c_3^{\pm} \frac{\partial^2 w^{\pm}}{\partial x \partial y} - c_4^{\pm} \frac{\partial w^{\pm}}{\partial y} + c_1^{\pm} \kappa_{\pm}^2 w^{\pm} = 0 \quad \text{in } D_{\pm}, \tag{3.1}$$

where

$$\begin{aligned} c_1^{\pm} &= (y_{\pm} - f)^2, \\ c_2^{\pm} &= [f'(y_{\pm} - y)]^2 + y_{\pm}^2, \\ c_3^{\pm} &= 2f'(y_{\pm} - y)(y_{\pm} - f), \\ c_4^{\pm} &= (y_{\pm} - y)[f''(y_{\pm} - f) + 2(f')^2]. \end{aligned}$$

Correspondingly, the transparent boundary conditions (2.17) are changed into

$$\partial_y w^{\pm} \mp \left(1 - \frac{f}{y_{\pm}} \right) \left(T_{\pm} w^{\pm} + \rho^{\pm} \right) = 0 \quad \text{on } \Gamma_{\pm}, \tag{3.2}$$

and the continuity conditions (2.18) are reduced to

$$w^+(x, 0) = w^-(x, 0) \quad \text{and} \quad \left(\frac{y_+}{y_+ - f} \right) \partial_y w^+(x, 0) = \left(\frac{y_-}{y_- - f} \right) \partial_y w^-(x, 0). \tag{3.3}$$

The original scattering model problem is described by the homogeneous Helmholtz equation with a complex scattering surface. Under the change of variables, the curved scattering surface is reduced to a flat surface, but the Helmholtz equation is transformed into a complicated partial differential equation with variable coefficients. Next we consider a classical boundary perturbation method to reduce the complicated equation (3.1) into a sequence of the nonhomogeneous Helmholtz equations, which can be solved in an efficient manner.

3.2. Power series. Recalling $f = \varepsilon g$ in (2.1), we consider formal expansions of the fields $w^{\pm}$ in power series of the surface deformation parameter ε:

$$w^{\pm}(x, y; \varepsilon) = \sum_{n=0}^{\infty} w_n^{\pm}(x, y)\varepsilon^n. \tag{3.4}$$

Substituting (2.1) and (3.4) into (3.1), and grouping terms in power of ε, we may derive recursion equations for $w_n^{\pm}$:

$$\frac{\partial^2 w_n^{\pm}}{\partial x^2} + \frac{\partial^2 w_n^{\pm}}{\partial y^2} + \kappa_{\pm}^2 w_n^{\pm} = v_n^{\pm} \quad \text{in } D_{\pm}, \tag{3.5}$$

where

$$\begin{aligned} v_n^{\pm} =& \frac{2g}{y_{\pm}} \frac{\partial^2 w_{n-1}^{\pm}}{\partial x^2} + \frac{2g'(y_{\pm} - y)}{y_{\pm}} \frac{\partial^2 w_{n-1}^{\pm}}{\partial x \partial y} + \frac{g''(y_{\pm} - y)}{y_{\pm}} \frac{\partial w_{n-1}^{\pm}}{\partial y} + \frac{2\kappa_{\pm}^2 g}{y_{\pm}} w_{n-1}^{\pm} \\ & - \frac{g^2}{y_{\pm}^2} \frac{\partial^2 w_{n-2}^{\pm}}{\partial x^2} - \frac{(g')^2 (y_{\pm} - y)^2}{y_{\pm}^2} \frac{\partial^2 w_{n-2}^{\pm}}{\partial y^2} - \frac{2gg'(y_{\pm} - y)}{y_{\pm}^2} \frac{\partial^2 w_{n-2}^{\pm}}{\partial x \partial y} \\ & + \frac{[2(g')^2 - gg''](y_{\pm} - y)}{y_{\pm}^2} \frac{\partial w_{n-2}^{\pm}}{\partial y} - \frac{\kappa_{\pm}^2 g^2}{y_{\pm}^2} w_{n-2}^{\pm}, \quad n = 0, 1, \ldots. \end{aligned} \tag{3.6}$$

Substituting (2.1) and (3.4) into (3.2) yields boundary conditions for $w_n^{\pm}$:

$$\partial_y w_n^{\pm} \mp T_{\pm} w_n^{\pm} = \phi_n^{\pm} \quad \text{on } y = y_{\pm}, \tag{3.7}$$

where

$$\phi_0^+ = \phi^+, \quad \phi_1^+ = -\left(\frac{g}{y_+}\right) \partial_y w_0^+, \quad \phi_n^+ = -\left(\frac{g}{y_+}\right) T_+ w_{n-1}^+, \quad n = 2, 3, \ldots, \tag{3.8}$$

$$\phi_0^- = 0, \quad \phi_n^- = \left(\frac{g}{y_-}\right) T_- w_{n-1}^-, \quad n = 1, 2, \ldots. \tag{3.9}$$

Inserting (2.1) and (3.4) into (3.3) gives continuity conditions

$$w_n^+(x, 0) - w_n^-(x, 0) = 0 \quad \text{and} \quad \partial_y w_n^+(x, 0) - \partial_y w_n^-(x, 0) = \psi_n, \tag{3.10}$$

where

$$\psi_n = \left(\frac{g}{y_-}\right) \partial_y w_{n-1}^+ - \left(\frac{g}{y_+}\right) \partial_y w_{n-1}^-, \quad n = 0, 1, \ldots. \tag{3.11}$$

In all of the above recursions, it is understood that $w_n^{\pm}, v_n^{\pm}, \phi_n^{\pm}$, and ψ_n are denoted as zeros whenever the integer $n < 0$. We notice that the transmission problem (3.5)–(3.10) for the current terms $w_n^{\pm}$ involves some nonhomogeneous terms $v_n^{\pm}$, $\phi_n^{\pm}$, and ψ_n, which depend only on the previous two terms $w_{n-1}^{\pm}$ and $w_{n-1}^{\pm}$. Thus, the problem (3.5)–(3.11) in rectangular domains $D_{\pm}$ indeed can be solved efficiently in a recursive manner starting from $n = 0$.

Numerically, one of the main difficulties in solving the transmission problem (3.5)–(3.10) is how to treat the nonlocal boundary conditions in (3.7). Evidently, the boundary conditions (3.7) are local in the Fourier frequency space after taking the Fourier transform with respect to x. Taking the Fourier transform of (3.5) with respect to x, we obtain one-dimensional ordinary differential equations:

$$\frac{\partial^2 \hat{w}_n^+}{\partial y^2} + \eta_+^2 \hat{w}_n^+ = \hat{v}_n^+, \quad 0 < y < y_+, \tag{3.12}$$

$$\frac{\partial^2 \hat{w}_n^-}{\partial y^2} + \eta_-^2 \hat{w}_n^- = \hat{v}_n^-, \quad y_- < y < 0, \tag{3.13}$$

where η_+ and η_- are defined in (2.10) and (2.13), respectively. Importantly, the nonlocal boundary conditions (3.7) become local in the Fourier variable ξ:

$$\partial_y \hat{w}_n^+ - \mathrm{i}\eta_+ \hat{w}_n^+ = \hat{\phi}_n^+ \quad \text{on } y = y_+, \tag{3.14}$$

$$\partial_y \hat{w}_n^- + \mathrm{i}\eta_- \hat{w}_n^- = \hat{\phi}_n^- \quad \text{on } y = y_-. \tag{3.15}$$

The continuity conditions (3.10) reduce to

$$\hat{w}_n^+(\xi, 0) - \hat{w}_n^-(\xi, 0) = 0 \quad \text{and} \quad \partial_y \hat{w}_n^+(\xi, 0) - \partial_y \hat{w}_n^-(\xi, 0) = \hat{\psi}_n. \tag{3.16}$$

In the frequency domain, the two-dimensional transmission problem (3.5)–(3.11) reduces to a simple one-dimensional two-point boundary value problem (3.12)–(3.16). As is discussed in Appendix B, two-point boundary value problems can be solved analytically. Next we present an explicit solution for the problem (3.12)–(3.11).

Considering the second order equation (3.12) along with the boundary condition (3.14), we may deduce from Theorem B.1 that the solution can be represented as

$$\hat{w}_n^+(\xi, y) = e^{\mathrm{i}\eta_+ y} \hat{w}_n^+(\xi, 0) + K_1^+(\xi, y)\hat{\phi}_n^+(\xi) - \int_0^{y_+} K_2^+(\xi, y, z)\hat{v}_n^+(\xi, z)dz, \tag{3.17}$$

where

$$K_1^+(\xi, y) = \frac{e^{\mathrm{i}\eta_+ y_+}}{2\mathrm{i}\eta_+} \left(e^{\mathrm{i}\eta_+ y} - e^{-\mathrm{i}\eta_+ y}\right) \tag{3.18}$$

and

$$K_2^+(\xi, y, z) = \begin{cases} \dfrac{e^{\mathrm{i}\eta_+ y}}{2\mathrm{i}\eta_+} \left(e^{\mathrm{i}\eta_+ z} - e^{-\mathrm{i}\eta_+ z}\right), & z < y, \\ \dfrac{e^{\mathrm{i}\eta_+ z}}{2\mathrm{i}\eta_+} \left(e^{\mathrm{i}\eta_+ y} - e^{-\mathrm{i}\eta_+ y}\right), & z > y. \end{cases} \tag{3.19}$$

Similarly, we may apply Theorem B.2 to the second order equation (3.13) along with the boundary condition (3.15), and derive that the solution is given as

$$\hat{w}_n^-(\xi,y) = e^{-\mathrm{i}\eta_- y}\hat{w}_n^-(\xi,0) + K_1^-(\xi,y)\hat{\phi}_n^-(\xi) + \int_{y_-}^0 K_2^-(\xi,y,z)\hat{v}_n^-(\xi,z)dz, \tag{3.20}$$

where

$$K_1^-(\xi,y) = \frac{e^{-\mathrm{i}\eta_- y_-}}{2\mathrm{i}\eta_-}\left(e^{\mathrm{i}\eta_- y} - e^{-\mathrm{i}\eta_- y}\right) \tag{3.21}$$

and

$$K_2^-(\xi,y,z) = \begin{cases} \dfrac{e^{-\mathrm{i}\eta_- z}}{2\mathrm{i}\eta_-}\left(e^{\mathrm{i}\eta_- y} - e^{-\mathrm{i}\eta_- y}\right), & z < y, \\ \dfrac{e^{-\mathrm{i}\eta_- y}}{2\mathrm{i}\eta_-}\left(e^{\mathrm{i}\eta_- z} - e^{-\mathrm{i}\eta_- z}\right), & z > y. \end{cases} \tag{3.22}$$

In (3.17) and (3.20), the solutions are given in terms of $\hat{w}_n^\pm(\xi,0)$, which are unknown but can be determined from the continuity conditions (3.16). Indeed, simple calculations yield

$$\partial_y \hat{w}_n^+(\xi,0) = \mathrm{i}\eta_+\hat{w}_n^+(\xi,0) + e^{\mathrm{i}\eta_+ y_+}\hat{\phi}_n^+(\xi) - \int_0^{y_+} e^{\mathrm{i}\eta_+ z}\hat{v}_n^+(\xi,z)dz,$$

$$\partial_y \hat{w}_n^-(\xi,0) = -\mathrm{i}\eta_-\hat{w}_n^-(\xi,0) + e^{-\mathrm{i}\eta_- y_-}\hat{\phi}_n^-(\xi) + \int_{y_-}^0 e^{-\mathrm{i}\eta_- z}\hat{v}_n^+(\xi,z)dz,$$

which combines with (3.16) to yield

$$\begin{aligned}\hat{w}_n^\pm(\xi,0) = &-\mathrm{i}(\eta_+ + \eta_-)^{-1}\Big[\hat{\psi}_n + e^{-\mathrm{i}\eta_- y_-}\hat{\phi}_n^- - e^{\mathrm{i}\eta_+ y_+}\hat{\phi}_n^+ \\ &+ \int_0^{y_+} e^{\mathrm{i}\eta_+ z}\hat{v}_n^+(\xi,z)dz + \int_{y_-}^0 e^{-\mathrm{i}\eta_- z}\hat{v}_n^-(\xi,z)dz\Big].\end{aligned} \tag{3.23}$$

Once $\hat{w}_n^\pm(\xi,y)$ are computed from (3.17)–(3.23), the solutions $w_n^\pm(x,y)$ can be obtained by taking the inverse Fourier transform of $\hat{w}_n^\pm(\xi,y)$ with respect to ξ.

4. Inverse problem.

In this section, we present an efficient and stable method for reconstructing the scattering surface from the transformed field expansion introduced in the previous section. Explicit reconstruction formulas are deduced for both the reflection configuration and the transmission configuration and are numerically realized by using the FFT.

4.1. Formulation.

The inverse surface scattering problem is nonlinear. Based on the power series (3.4), a linearization is considered in order to derive explicit reconstruction formulas.

Let $u^\delta(x,y_+)$ and $u^\delta(x,y_-)$ be the noisy data measured from the reflection configuration at Γ_+ and the transmission configuration at Γ_-, respectively. We assume that the data $u^\delta(x,y_\pm)$ takes the form

$$u^\delta(x,y_\pm) = u^\pm(x,y_\pm) + \mathcal{O}(\delta), \tag{4.1}$$

where $u^{\pm}(x, y_{\pm})$ denotes the noise-free data at $\Gamma_{\pm}$ and δ represents the noise level.

It follows from the asymptotic expansion (3.4) that we have

$$w^{\pm}(x, y) = w_0^{\pm}(x, y) + \varepsilon w_1^{\pm}(x, y) + \mathcal{O}(\varepsilon^2). \tag{4.2}$$

Evaluating (4.2) at $y = y_{\pm}$, and noting $w^{\pm}(x, y_{\pm}) = u^{\pm}(x, y_{\pm})$ and $w^{\delta}(x, y_{\pm}) = u^{\delta}(x, y_{\pm})$ under the change of variables, we have

$$w^{\delta}(x, y_{\pm}) = w_0^{\pm}(x, y_{\pm}) + \varepsilon w_1^{\pm}(x, y_{\pm}) + \mathcal{O}(\varepsilon^2) + \mathcal{O}(\delta). \tag{4.3}$$

Rearranging (4.3) yields

$$\varepsilon w_1^{\pm}(x, y_{\pm}) = \Big(w^{\delta}(x, y_{\pm}) - w_0^{\pm}(x, y_{\pm})\Big) + \mathcal{O}(\varepsilon^2) + \mathcal{O}(\delta), \tag{4.4}$$

which is the basis of our reconstruction formulas. Here the two parameters ε and δ indicate the ill-posed nature of the inverse problem: the larger the two parameters ε and δ are, the more severe the ill-posedness of the inverse problem is. Neglecting the asymptotic terms of ε^2 and δ in (4.4) gives

$$\varepsilon w_1^{\pm}(x, y_{\pm}) = w^{\delta}(x, y_{\pm}) - w_0^{\pm}(x, y_{\pm}), \tag{4.5}$$

which actually linearizes the nonlinear inverse problem and may lead to explicit inversion formulas for the linearized inverse problem.

In the rest of this section, using solution representations (3.17) and (3.20), we shall derive an analytic expression of the order zero term $w_0^{\pm}$, which represents the solution of a plane wave propagating in a two-layered medium, and the order one term $w_1^{\pm}$, which carries information of the scattering surface f.

4.2. Order zero. Recalling (3.6), (3.8), (3.9), and (3.11), we have

$$v_0^{\pm} = 0, \quad \phi_0^{+} = -2\mathrm{i}\beta_+ e^{\mathrm{i}(\alpha x - \beta_+ y_+)}, \quad \phi_0^{-} = 0, \quad \psi_0 = 0,$$

which give, after taking the Fourier transform with respect to x,

$$\hat{v}_0^{\pm} = 0, \quad \hat{\phi}_0^{+} = -2(2\pi)^{1/2}\mathrm{i}\beta_+ \delta(\xi - \alpha) e^{-\mathrm{i}\beta_+ y_+}, \quad \hat{\phi}_0^{-} = 0, \quad \hat{\psi}_0 = 0.$$

Here δ is the Dirac delta function.

Plugging the above quantities into (3.23), we obtain

$$\begin{aligned} \hat{w}_0^{\pm}(\xi, 0) = &-\mathrm{i}(\eta_+ + \eta_-)^{-1}\Big[\hat{\psi}_0 + e^{-\mathrm{i}\eta_- y_-}\hat{\phi}_0^{-} - e^{\mathrm{i}\eta_+ y_+}\hat{\phi}_0^{+} \\ &+ \int_0^{y_+} e^{\mathrm{i}\eta_+ z}\hat{v}_0^{+}(\xi, z)dz + \int_{y_-}^{0} e^{-\mathrm{i}\eta_- z}\hat{v}_0^{-}(\xi, z)dz\Big] = \left(\frac{\mathrm{i}e^{\mathrm{i}\eta_+ y_+}}{\eta_+ + \eta_-}\right)\hat{\phi}_0^{+}. \end{aligned} \tag{4.6}$$

Using the solution representations (3.17) and (3.20), we have

$$\hat{w}_0^{+}(\xi, y) = e^{\mathrm{i}\eta_+ y}\hat{w}_0^{+}(\xi, 0) + K_1^{+}(\xi, y)\hat{\phi}_0^{+}(\xi) \tag{4.7}$$

and

$$\hat{w}_0^-(\xi, y) = e^{-\mathrm{i}\eta_- y}\hat{w}_0^-(\xi, 0). \tag{4.8}$$

Substituting (4.6) into (4.7) and (4.8) yields

$$\hat{w}_0^+(\xi, y) = \left(\frac{\mathrm{i}e^{\mathrm{i}\eta_+ y_+}}{\eta_+ + \eta_-}\right) e^{\mathrm{i}\eta_+ y}\hat{\phi}_0^+ + \left(\frac{e^{\mathrm{i}\eta_+ y_+}}{2\mathrm{i}\eta_+}\right)\left(e^{\mathrm{i}\eta_+ y} - e^{-\mathrm{i}\eta_+ y}\right)\hat{\phi}_0^+ \tag{4.9}$$

and

$$\hat{w}_0^-(\xi, y) = \left(\frac{\mathrm{i}e^{\mathrm{i}\eta_+ y_+}}{\eta_+ + \eta_-}\right) e^{-\mathrm{i}\eta_- y}\hat{\phi}_0^+. \tag{4.10}$$

It can be verified from (2.10) that $\eta_+(\alpha) = \beta_+$. Denote $\beta_- = \eta_-(\alpha)$. Plugging $\hat{\phi}_0^+$ into (4.9) and (4.10), and taking the inverse Fourier transform, we obtain

$$\begin{aligned} w_0^+(x, y) &= \int_{\mathbb{R}} \left(\frac{2\beta_+}{\eta_+ + \eta_-}\right) \delta(\xi - \alpha) e^{\mathrm{i}\eta_+ y} e^{\mathrm{i}\xi x} d\xi \\ &\quad - \int_{\mathbb{R}} \left(\frac{\beta_+}{\eta_+}\right) \delta(\xi - \alpha)(e^{\mathrm{i}\eta_+ y} - e^{-\mathrm{i}\eta_+ y}) e^{\mathrm{i}\xi x} d\xi \\ &= \left(\frac{2\beta_+}{\beta_+ + \beta_-}\right) e^{\mathrm{i}(\alpha x + \beta_+ y)} + e^{\mathrm{i}\alpha x}(e^{-\mathrm{i}\beta_+ y} - e^{\mathrm{i}\beta_+ y}) = e^{\mathrm{i}(\alpha x - \beta_+ y)} + re^{\mathrm{i}(\alpha x + \beta_+ y)} \end{aligned} \tag{4.11}$$

and

$$w_0^-(x, y) = \int_{\mathbb{R}} \left(\frac{2\beta_+}{\eta_+ + \eta_-}\right) \delta(\xi - \alpha) e^{-\mathrm{i}\eta_- y} e^{\mathrm{i}\xi x} d\xi = te^{\mathrm{i}(\alpha x - \beta_- y)}, \tag{4.12}$$

where

$$r = \frac{\beta_+ - \beta_-}{\beta_+ + \beta_-} \quad \text{and} \quad t = \frac{2\beta_+}{\beta_+ + \beta_-} \tag{4.13}$$

are known as the reflection coefficient and the transmission coefficient, respectively.

Denote

$$u^{\mathrm{ref}}(x, y) = re^{\mathrm{i}(\alpha x + \beta_+ y)} \quad \text{and} \quad u^{\mathrm{tra}}(x, y) = te^{\mathrm{i}(\alpha x - \beta_- y)}.$$

Clearly, u^{ref} and u^{tra} represent the reflected plane wave and the transmitted plane wave, respectively. The leading term w_0^+ consists of the incident field and the reflected field, i.e., $w_0^+ = u^{\mathrm{inc}} + u^{\mathrm{ref}}$, and the leading term w_0^- is the transmitted field, i.e., $w_0^- = u^{\mathrm{tra}}$.

Physically, the leading term $w_0^\pm$ arises from the interaction between the incident field u^{inc} and the plane dielectric surface, which generate the reflected field u^{ref} and the transmitted field u^{tra}. Mathematically, they satisfy the Helmholtz equation

$$\Delta w_0^\pm + \kappa_\pm^2 w_0^\pm = 0 \quad \text{in } D_\pm,$$

along with the transparent boundary conditions

$$\partial_y w_0^\pm \mp T_\pm w_0^\pm = \phi^\pm \quad \text{on } \Gamma_\pm$$

and the continuity conditions

$$w_0^+(x, 0) = w_0^-(x, 0) \quad \text{and} \quad \partial_y w_0^+(x, 0) = \partial_y w_0(x, 0).$$

Indeed, it can be verified that the solutions $w_0^\pm$ are given in (4.11) and (4.12).

4.3. Order one. Recalling (3.11), (4.11), and (4.12), we have from simple calculations that

$$\psi_1(x) = \left(\frac{g}{y_-}\right)\partial_y w_0^+(x,0) - \left(\frac{g}{y_+}\right)\partial_y w_0^-(x,0) = \left[\frac{\mathrm{i}\beta_- t}{y_+} - \frac{\mathrm{i}\beta_+(1-r)}{y_-}\right] g(x)e^{\mathrm{i}\alpha x},$$

which gives, after taking the Fourier transform with respect to x,

$$\hat{\psi}_1(\xi) = \left[\frac{\mathrm{i}\beta_- t}{y_+} - \frac{\mathrm{i}\beta_+(1-r)}{y_-}\right]\hat{g}(\xi-\alpha). \tag{4.14}$$

Following (3.8)–(3.9) and (4.11)–(4.12), we have

$$\begin{aligned}\phi_1^+(x) &= -\left(\frac{g}{y_+}\right)(T_+ w_0^+ + \phi^+)(x,y_+) = -\left(\frac{g}{y_+}\right)\partial_y w_0^+(x,y_+)\\ &= \left(\frac{\mathrm{i}\beta_+}{y_+}\right)(e^{-\mathrm{i}\beta_+ y_+} - re^{\mathrm{i}\beta_+ y_+})g(x)e^{\mathrm{i}\alpha x}\end{aligned}$$

and

$$\begin{aligned}\phi_1^-(x) &= \left(\frac{g}{y_-}\right)(T_- w_0^-)(x,y_-) = -\left(\frac{g}{y_-}\right)\partial_y w_0^-(x,y_-)\\ &= \left(\frac{\mathrm{i}\beta_- t}{y_-}\right)e^{-\mathrm{i}\beta_- y_-} g(x)e^{\mathrm{i}\alpha x}.\end{aligned}$$

Taking the Fourier transform of ϕ_1^+ and ϕ_1^-, we obtain

$$\hat{\phi}_1^+(\xi) = \left(\frac{\mathrm{i}\beta_+}{y_+}\right)(e^{-\mathrm{i}\beta_+ y_+} - re^{\mathrm{i}\beta_+ y_+})\hat{g}(\xi-\alpha), \tag{4.15}$$

$$\hat{\phi}_1^-(\xi) = \left(\frac{\mathrm{i}\beta_- t}{y_-}\right)e^{-\mathrm{i}\beta_- y_-}\hat{g}(\xi-\alpha). \tag{4.16}$$

It follows from (3.6) that

$$v_1^\pm = \frac{2g}{y_\pm}\frac{\partial^2 w_0^\pm}{\partial x^2} + \frac{2g'(y_\pm - y)}{y_\pm}\frac{\partial^2 w_0^\pm}{\partial x \partial y} + \frac{g''(y_\pm - y)}{y_\pm}\frac{\partial w_0^\pm}{\partial y} + \frac{2\kappa_\pm^2 g}{y_\pm}w_0^\pm.$$

Substituting the expressions of $w_0^\pm$ in (4.11) and (4.12) into the right-hand side of the above equation and noting the definitions of $\beta_\pm$, we obtain

$$\begin{aligned}v_1^+ &= -\left(\frac{2\alpha^2}{y_+}\right)(e^{-\mathrm{i}\beta_+ y} + re^{\mathrm{i}\beta_+ y})g(x)e^{\mathrm{i}\alpha x} + \left(\frac{2\alpha\beta_+}{y_+}\right)(y_+ - y)(e^{-\mathrm{i}\beta_+ y} - re^{\mathrm{i}\beta_+ y})g'(x)e^{\mathrm{i}\alpha x}\\ &\quad - \left(\frac{\mathrm{i}\beta_+}{y_+}\right)(y_+ - y)(e^{-\mathrm{i}\beta_+ y} - re^{\mathrm{i}\beta_+ y})g''(x)e^{\mathrm{i}\alpha x} + \left(\frac{2\kappa_+^2}{y_+}\right)(e^{-\mathrm{i}\beta_+ y} + re^{\mathrm{i}\beta_+ y})g(x)e^{\mathrm{i}\alpha x}\\ &= \left(\frac{2\beta_+^2}{y_+}\right)(e^{-\mathrm{i}\beta_+ y} + re^{\mathrm{i}\beta_+ y})g(x)e^{\mathrm{i}\alpha x} + \left(\frac{2\alpha\beta_+}{y_+}\right)(y_+ - y)(e^{-\mathrm{i}\beta_+ y} - re^{\mathrm{i}\beta_+ y})g'(x)e^{\mathrm{i}\alpha x}\\ &\quad - \left(\frac{\mathrm{i}\beta_+}{y_+}\right)(y_+ - y)(e^{-\mathrm{i}\beta_+ y} - re^{\mathrm{i}\beta_+ y})g''(x)e^{\mathrm{i}\alpha x}\end{aligned}$$

and

$$\begin{aligned} v_1^- =& -\left(\frac{2\alpha^2 t}{y_-}\right) e^{-\mathrm{i}\beta_- y} g(x) e^{\mathrm{i}\alpha x} + \left(\frac{2\alpha\beta_- t}{y_-}\right)(y_- - y) e^{-\mathrm{i}\beta_- y} g'(x) e^{\mathrm{i}\alpha x} \\ & - \left(\frac{\mathrm{i}\beta_- t}{y_-}\right)(y_- - y) e^{-\mathrm{i}\beta_- y} g''(x) e^{\mathrm{i}\alpha x} + \left(\frac{2\kappa_-^2 t}{y_-}\right) e^{-\mathrm{i}\beta_- y} g(x) e^{\mathrm{i}\alpha x} \\ =& \left(\frac{2\beta_-^2 t}{y_-}\right) e^{-\mathrm{i}\beta_- y} g(x) e^{\mathrm{i}\alpha x} + \left(\frac{2\alpha\beta_- t}{y_-}\right)(y_- - y) e^{-\mathrm{i}\beta_- y} g'(x) e^{\mathrm{i}\alpha x} \\ & - \left(\frac{\mathrm{i}\beta_- t}{y_-}\right)(y_- - y) e^{-\mathrm{i}\beta_- y} g''(x) e^{\mathrm{i}\alpha x}. \end{aligned}$$

Taking the Fourier transform of $v_1^{\pm}$ yields

$$\begin{aligned} \hat{v}_1^+(\xi, y) = \Bigg[& \left(\frac{2\beta_+^2}{y_+}\right)(e^{-\mathrm{i}\beta_+ y} + r e^{\mathrm{i}\beta_+ y}) + \left(\frac{2\mathrm{i}\xi\alpha\beta_+}{y_+}\right)(y_+ - y)(e^{-\mathrm{i}\beta_+ y} - r e^{\mathrm{i}\beta_+ y}) \\ & + \left(\frac{\mathrm{i}\xi^2\beta_+}{y_+}\right)(y_+ - y)(e^{-\mathrm{i}\beta_+ y} - r e^{\mathrm{i}\beta_+ y})\Bigg] \hat{g}(\xi - \alpha) \end{aligned} \tag{4.17}$$

and

$$\begin{aligned} \hat{v}_1^-(\xi, y) = \Bigg[& \left(\frac{2\beta_-^2 t}{y_-}\right) e^{-\mathrm{i}\beta_- y} + \left(\frac{2\mathrm{i}\xi\alpha\beta_- t}{y_-}\right)(y_- - y) e^{-\mathrm{i}\beta_- y} \\ & + \left(\frac{\mathrm{i}\xi^2\beta_- t}{y_-}\right)(y_- - y) e^{-\mathrm{i}\beta_- y}\Bigg] \hat{g}(\xi - \alpha). \end{aligned} \tag{4.18}$$

To simplify tedious calculations, from now on, we consider the special case of a normal incidence for the incident field, i.e.,

$$\theta = 0, \quad \alpha = 0, \quad \beta_\pm = \kappa_\pm.$$

Otherwise, there is a phase shift of the reconstruction for other directions of incidence due to $\alpha \neq 0$.

Under the normal incidence, (4.14) reduces to

$$\hat{\psi}_1(\xi) = \left[\frac{\mathrm{i}\kappa_- t}{y_+} - \frac{\mathrm{i}\kappa_+(1-r)}{y_-}\right] \hat{g}(\xi), \tag{4.19}$$

(4.15) and (4.16) can be written as

$$\hat{\phi}_1^+(\xi) = \left(\frac{\mathrm{i}\kappa_+}{y_+}\right)(e^{-\mathrm{i}\kappa_+ y_+} - r e^{\mathrm{i}\kappa_+ y_+}) \hat{g}(\xi), \tag{4.20}$$

$$\hat{\phi}_1^-(\xi) = \left(\frac{\mathrm{i}\kappa_- t}{y_-}\right) e^{-\mathrm{i}\kappa_- y_-} \hat{g}(\xi), \tag{4.21}$$

and (4.17) and (4.18) are simplified to

$$\hat{v}_1^+(\xi,y) = \left[\left(\frac{2\kappa_+^2}{y_+}\right)(e^{-\mathrm{i}\kappa_+ y} + re^{\mathrm{i}\kappa_+ y}) + \left(\frac{\mathrm{i}\xi^2\kappa_+}{y_+}\right)(y_+ - y)(e^{-\mathrm{i}\kappa_+ y} - re^{\mathrm{i}\kappa_+ y})\right]\hat{g}(\xi), \tag{4.22}$$

$$\hat{v}_1^-(\xi,y) = \left[\left(\frac{2\kappa_-^2 t}{y_-}\right)e^{-\mathrm{i}\kappa_- y} + \left(\frac{\mathrm{i}\xi^2\kappa_- t}{y_-}\right)(y_- - y)e^{-\mathrm{i}\kappa_- y}\right]\hat{g}(\xi). \tag{4.23}$$

Correspondingly, the reflection coefficient r and the transmission coefficient t are reduced to

$$r = \frac{\kappa_+ - \kappa_-}{\kappa_+ + \kappa_-} \quad \text{and} \quad t = \frac{2\kappa_+}{\kappa_+ + \kappa_-}. \tag{4.24}$$

It follows from (3.23) that

$$\begin{aligned}\hat{w}_1^{\pm}(\xi,0) =& -\mathrm{i}(\eta_+ + \eta_-)^{-1}\Big[\hat{\psi}_1 + e^{-\mathrm{i}\eta_- y_-}\hat{\phi}_1^- - e^{\mathrm{i}\eta_+ y_+}\hat{\phi}_1^+ + \int_0^{y_+} e^{\mathrm{i}\eta_+ z}\hat{v}_1^+(\xi,z)dz \\ &+ \int_{y_-}^0 e^{-\mathrm{i}\eta_- z}\hat{v}_1^-(\xi,z)dz\Big] \\ =& -\mathrm{i}(\eta_+ + \eta_-)^{-1}(M_1 + M_2 + M_3).\end{aligned} \tag{4.25}$$

Next we compute M_1, M_2, and M_3 explicitly in order to simplify the expression of $\hat{w}_1^{\pm}(\xi,0)$.

Noting (4.19)–(4.21), we get

$$\begin{aligned}M_1 =& \hat{\psi}_1 + e^{-\mathrm{i}\eta_- y_-}\hat{\phi}_1^- - e^{\mathrm{i}\eta_+ y_+}\hat{\phi}_1^+ \\ =& \left[\frac{\mathrm{i}\kappa_- t}{y_+} - \frac{\mathrm{i}\kappa_+(1-r)}{y_-}\right]\hat{g}(\xi) + \left(\frac{\mathrm{i}\kappa_- t}{y_-}\right)e^{-\mathrm{i}(\eta_- + \kappa_-)y_-}\hat{g}(\xi) \\ &- \left(\frac{\mathrm{i}\kappa_+}{y_+}\right)e^{\mathrm{i}\eta_+ y_+}(e^{-\mathrm{i}\kappa_+ y_+} - re^{\mathrm{i}\kappa_+ y_+})\hat{g}(\xi).\end{aligned} \tag{4.26}$$

Using (4.22) and (4.23), we have from integration by parts that

$$\begin{aligned}M_2 =& \int_0^{y_+} e^{\mathrm{i}\eta_+ z}\hat{v}_1^+(\xi,z)dz = \int_0^{y_+} e^{\mathrm{i}\eta_+ z}\left[\left(\frac{2\kappa_+^2}{y_+}\right)(e^{-\mathrm{i}\kappa_+ z} + re^{\mathrm{i}\kappa_+ z}) \right.\\ &\left. + \left(\frac{\mathrm{i}\xi^2\kappa_+}{y_+}\right)(y_+ - z)(e^{-\mathrm{i}\kappa_+ z} - re^{\mathrm{i}\kappa_+ z})\right]\hat{g}(\xi)dz \\ =& \left(\frac{2\mathrm{i}\kappa_+^2}{y_+}\right)\left[\frac{\left(1 - e^{\mathrm{i}(\eta_+ - \kappa_+)y_+}\right)}{(\eta_+ - \kappa_+)} + \frac{r\left(1 - e^{\mathrm{i}(\eta_+ + \kappa_+)y_+}\right)}{(\eta_+ + \kappa_+)}\right]\hat{g}(\xi) \\ &- \xi^2\kappa_+\left[\frac{1}{(\eta_+ - \kappa_+)} - \frac{r}{(\eta_+ + \kappa_+)}\right]\hat{g}(\xi)\end{aligned}$$

$$+\left(\frac{\mathrm{i}\xi^2\kappa_+}{y_+}\right)\left[\frac{\left(1-e^{\mathrm{i}(\eta_+-\kappa_+)y_+}\right)}{(\eta_+-\kappa_+)^2}-\frac{r\left(1-e^{\mathrm{i}(\eta_++\kappa_+)y_+}\right)}{(\eta_++\kappa_+)^2}\right]\hat{g}(\xi)$$

$$=\left(\frac{\mathrm{i}\kappa_+}{y_+}\right)e^{\mathrm{i}\eta_+y_+}(e^{-\mathrm{i}\kappa_+y_+}-re^{\mathrm{i}\kappa_+y_+})\hat{g}(\xi)-\left[\frac{\mathrm{i}\kappa_+(1-r)}{y_+}\right]\hat{g}(\xi)$$

$$+\left[\kappa_+(\eta_++\kappa_+)-r\kappa_+(\eta_+-\kappa_+)\right]\hat{g}(\xi) \tag{4.27}$$

and

$$M_3=\int_{y_-}^0 e^{-\mathrm{i}\eta_-z}\hat{v}_1^-(\xi,z)dz=\int_{y_-}^0 e^{-\mathrm{i}\eta_-z}\left[\left(\frac{2\kappa_-^2t}{y_-}\right)e^{-\mathrm{i}\kappa_-z}\right.$$

$$\left.+\left(\frac{\mathrm{i}\xi^2\kappa_-t}{y_-}\right)(y_--z)e^{-\mathrm{i}\kappa_-z}\right]\hat{g}(\xi)dz$$

$$=\left(\frac{2\mathrm{i}\kappa_-^2t}{y_-}\right)\left(\frac{1-e^{-\mathrm{i}(\eta_-+\kappa_-)y_-}}{(\eta_-+\kappa_-)}\right)\hat{g}(\xi)-\frac{\xi^2\kappa_-t}{(\eta_-+\kappa_-)}\hat{g}(\xi)$$

$$-\left(\frac{\mathrm{i}\xi^2\kappa_-t}{y_-}\right)\left(\frac{1-e^{-\mathrm{i}(\eta_-+\kappa_-)y_-}}{(\eta_-+\kappa_-)^2}\right)\hat{g}(\xi)$$

$$=\left(\frac{\mathrm{i}\kappa_-t}{y_-}\right)\left(1-e^{-\mathrm{i}(\eta_-+\kappa_-)y_-}\right)\hat{g}(\xi)+t\kappa_-(\eta_--\kappa_-)\hat{g}(\xi). \tag{4.28}$$

Noting $\kappa_+(1-r)=\kappa_-t$ due to (4.24) and combining (4.26)–(4.28), we can simplify (4.25) to

$$\hat{w}_1^{\pm}(\xi,0)=C_0(\xi,\kappa_\pm)\hat{g}(\xi), \tag{4.29}$$

where

$$C_0(\xi,\kappa_\pm)=-\mathrm{i}(\eta_++\eta_-)^{-1}\left[\kappa_+(\eta_++\kappa_+)-r\kappa_+(\eta_+-\kappa_+)+t\kappa_-(\eta_--\kappa_-)\right]. \tag{4.30}$$

It follows from the solution representation (3.17) that

$$\hat{w}_1^+(\xi,y)=N_1^+(\xi,y)+N_2^+(\xi,y)-N_3^+(\xi,y), \tag{4.31}$$

where

$$N_1^+=e^{\mathrm{i}\eta_+y}\hat{w}_1^+(\xi,0),\quad N_2^+=K_1^+(\xi,y)\hat{\phi}_1^+(\xi),\quad N_3^+=\int_0^{y_+}K_2^+(\xi,y,z)\hat{v}_1^+(\xi,z)dz.$$

Evaluating (4.31) at $y=y_+$ yields

$$\hat{w}_1^+(\xi,y_+)=N_1^+(\xi,y_+)+N_2^+(\xi,y_+)-N_3^+(\xi,y_+).$$

Simple calculations yield

$$N_1^+(\xi,y_+)=C_0(\xi,\kappa_+,\kappa_-)e^{\mathrm{i}\eta_+y_+}\hat{g}(\xi). \tag{4.32}$$

Using (4.20), we have

$$N_2^+(\xi, y_+) = K_1^+(\xi, y_+)\hat{\phi}_1^+(\xi)$$

$$= \left(\frac{\kappa_+}{2\eta_+ y_+}\right)\left(e^{\mathrm{i}(\eta_+ - \kappa_+)y_+} - re^{\mathrm{i}(\eta_+ + \kappa_+)y_+}\right)(e^{\mathrm{i}\eta_+ y_+} - e^{-\mathrm{i}\eta_+ y_+})\hat{g}(\xi). \tag{4.33}$$

Following the definitions of K_2^+ and v_1^+, and using the same integration by parts as for M_2, we obtain

$$N_3^+(\xi, y_+) = \int_0^{y_+} K_2^+(\xi, y_+, z)\hat{v}_1^+(\xi, z)dz = \int_0^{y_+} \frac{e^{\mathrm{i}\eta_+ y_+}}{2\mathrm{i}\eta_+}(e^{\mathrm{i}\eta_+ z} - e^{-\mathrm{i}\eta_+ z})$$

$$\times \left[\left(\frac{2\kappa_+^2}{y_+}\right)(e^{-\mathrm{i}\kappa_+ z} + re^{\mathrm{i}\kappa_+ z}) + \left(\frac{\mathrm{i}\xi^2\kappa_+}{y_+}\right)(y_+ - z)(e^{-\mathrm{i}\kappa_+ z} - re^{\mathrm{i}\kappa_+ z})\right]\hat{g}(\xi)dz$$

$$= \left(\frac{\kappa_+}{2\eta_+ y_+}\right)\left(e^{\mathrm{i}(\eta_+ - \kappa_+)y_+} - re^{\mathrm{i}(\eta_+ + \kappa_+)y_+}\right)(e^{\mathrm{i}\eta_+ y_+} - e^{-\mathrm{i}\eta_+ y_+})\hat{g}(\xi)$$

$$- \mathrm{i}\kappa_+(1 - r)e^{\mathrm{i}\eta_+ y_+}\hat{g}(\xi). \tag{4.34}$$

Combining (4.32)–(4.34) yields

$$\hat{w}_1^+(\xi, y_+) = C_+(\xi, \kappa_\pm)e^{\mathrm{i}\eta_+ y_+}\hat{g}(\xi), \tag{4.35}$$

where

$$C_+(\xi, \kappa_\pm) = C_0(\xi, \kappa_\pm) + \mathrm{i}\kappa_+(1 - r). \tag{4.36}$$

It follows from the solution representation (3.20) that

$$\hat{w}_1^-(\xi, y) = N_1^-(\xi, y) + N_2^-(\xi, y) + N_3^-(\xi, y), \tag{4.37}$$

where

$$N_1^- = e^{-\mathrm{i}\eta_- y}\hat{w}_1^-(\xi, 0), \quad N_2^- = K_1^-(\xi, y)\hat{\phi}_1^-(\xi), \quad N_3^- = \int_{y_-}^0 K_2^-(\xi, y, z)\hat{v}_1^-(\xi, z)dz.$$

Evaluating (4.37) at $y = y_-$ yields

$$\hat{w}_1^-(\xi, y_-) = N_1^-(\xi, y_-) + N_2^-(\xi, y_-) + N_3^-(\xi, y_-).$$

Simple calculations yield

$$N_1^-(\xi, y_-) = C_0(\xi, \kappa_\pm)e^{-\mathrm{i}\eta_- y_-}\hat{g}(\xi). \tag{4.38}$$

Using (4.21), we have

$$N_2^-(\xi, y_-) = K_1^-(\xi, y_-)\hat{\phi}_1^-(\xi)$$

$$= \left(\frac{\kappa_- t}{2\eta_- y_-}\right) e^{-\mathrm{i}(\eta_- + \kappa_-)y_-}(e^{\mathrm{i}\eta_- y_-} - e^{-\mathrm{i}\eta_- y_-})\hat{g}(\xi). \tag{4.39}$$

Following the definitions of K_2^- and v_1^-, and using the same integration by parts as for M_3, we get

$$N_3^-(\xi, y_-) = \int_{y_-}^0 K_2^-(\xi, y_-, z)\hat{v}_1^-(\xi, z)dz = \int_{y_-}^0 \frac{e^{-\mathrm{i}\eta_- y_-}}{2\mathrm{i}\eta_-}(e^{\mathrm{i}\eta_- z} - e^{-\mathrm{i}\eta_- z})$$
$$\times \left[\left(\frac{2\kappa_-^2 t}{y_-}\right) e^{-\mathrm{i}\kappa_- z} + \left(\frac{\mathrm{i}\xi^2\kappa_- t}{y_+}\right)(y_- - z)e^{-\mathrm{i}\kappa_- z}\right]dz$$
$$= -\left(\frac{\kappa_- t}{2\eta_- y_-}\right) e^{-\mathrm{i}(\eta_- + \kappa_-)y_-}(e^{\mathrm{i}\eta_- y_-} - e^{-\mathrm{i}\eta_- y_-})\hat{g}(\xi) + \mathrm{i}\kappa_- t\hat{g}(\xi). \tag{4.40}$$

Adding (4.38)–(4.40) yields

$$\hat{w}_1^-(\xi, y_-) = C_-(\xi, \kappa_\pm)e^{-\mathrm{i}\eta_- y_-}\hat{g}(\xi), \tag{4.41}$$

where

$$C_-(\xi, \kappa_\pm) = C_0(\xi, \kappa_\pm) + \mathrm{i}\kappa_- t. \tag{4.42}$$

Following from the definitions of the reflection coefficient r and the transmission coefficient t in (4.24), and (4.36) and (4.42), we may verify that

$$\kappa_+(1 - r) = \kappa_- t = \frac{2\kappa_+\kappa_-}{\kappa_+ + \kappa_-},$$

which gives

$$C_+(\xi, \kappa_\pm) = C_-(\xi, \kappa_\pm) \quad \text{for all } \xi \in \mathbb{R}.$$

Hence (4.35) and (4.41) can be written as

$$\hat{w}_1^\pm(\xi, y_\pm) = C(\xi, \kappa_\pm)e^{\pm\mathrm{i}\eta_\pm y_\pm}\hat{g}(\xi), \tag{4.43}$$

where

$$C(\xi, \kappa_\pm) = C_0(\xi, \kappa_\pm) + \left(\frac{2\mathrm{i}\kappa_+\kappa_-}{\kappa_+ + \kappa_-}\right). \tag{4.44}$$

As shown in (4.43), the first order term $\hat{w}_1^\pm(\xi, y_\pm)$ carries essential information of the scattering surface function f.

4.4. Reconstruction formulas. Taking the Fourier transform of (4.5), we have

$$\varepsilon\hat{w}_1^\pm(\xi, y_\pm) = \hat{w}^\delta(\xi, y_\pm) - \hat{w}_0^\pm(\xi, y_\pm). \tag{4.45}$$

Noting $\hat{f} = \varepsilon\hat{g}$, and combining (4.45) with (4.35) and (4.41), we deduce explicit inversion formulas to reconstruct the scattering surface function via the reflection configuration and the transmission configuration:

$$\hat{f}_{\varepsilon,\delta} = C^{-1}(\xi, \kappa_\pm)\left(\hat{w}^\delta(\xi, y_\pm) - \hat{w}_0^\pm(\xi, y_\pm)\right)e^{\mp\mathrm{i}\eta_\pm y_\pm}. \tag{4.46}$$

Here the subscripts ε and δ indicate the dependence of the reconstruction on these two parameters.

It is easily seen from the definitions of $\eta_\pm$ in (2.10) and (2.13) that the inversion formulas (4.46) make use of both propagation wave modes and evanescent wave modes. More explicitly, it follows from the definitions of $\eta_\pm$ that we have

$$\hat{f}_{\varepsilon,\delta} = C^{-1}(\xi,\kappa_\pm)\left(\hat{w}^\delta(\xi,y_\pm) - \hat{w}_0^\pm(\xi,y_\pm)\right) e^{\mp \mathrm{iRe}\,\eta_\pm(\xi)y_\pm}\, e^{\pm \mathrm{Im}\,\eta_\pm(\xi)y_\pm}. \tag{4.47}$$

Clearly, the low spatial frequency modes of the scattering surface function f come from the propagation waves, while the evanescent waves contribute to the high spatial frequency modes of the scattering surface function f, which do not obey the Rayleigh criterion and display superresolution.

As shown in (4.47), it is well-posed to reconstruct the scattering surface function for Fourier modes with $\mathrm{Im}\,\eta_\pm(\xi) = 0$ in the sense that small variations in the measured data will not lead to large errors in the reconstruction. Thus, no regularization is needed for the reconstruction formulas (4.47) for ξ such that $\mathrm{Im}\,\eta_\pm(\xi) = 0$. In contrast, it is severely ill-posed using (4.47) to reconstruct the scattering surface function for Fourier modes with $\mathrm{Im}\,\eta_\pm(\xi) > 0$. Small variations in the measured data will be exponentially amplified and lead to huge errors in the reconstruction. Thus, regularization must be considered to suppress the exponential growth of the reconstruction errors for the reconstruction formulas (4.47) corresponding to those ξ such that $\mathrm{Im}\,\eta_\pm(\xi) > 0$.

There are two ideas to remedy the ill-posedness of the inversion formulas (4.47) and thus obtain a stable and superresolved reconstruction. One idea is to make $|y_\pm|$ as small as possible, i.e., measure the data at the height which is as close as possible to the scattering surface. This is exactly the idea of near-field optics: by bringing a scanning tip into the near-field (subwavelength) of the sample, the high frequency evanescent field can be detected, and thus images with subwavelength resolution may be obtained. Another idea is to adopt a commonly used regularization technique such as spectral cut-off or Tikhonov regularization [27]. We do not discuss here the relative advantages or disadvantages of different regularization methods. Following [12, 24], we consider only the cut-off regularization. For a fixed measurement distance $|y_\pm|$, the cut-off frequency $\omega_\pm$ depends on the noise level δ and the surface deformation parameter ε. Define the signal-to-noise ratio (SNR) by

$$\mathrm{SNR} = \min\{\varepsilon^{-2},\ \delta^{-1}\},$$

which measures the noise level and the surface deformation parameter. We choose the cut-off frequencies $\omega_\pm$ in such a way that

$$e^{\pm \mathrm{Im}\,\eta_\pm(\omega_\pm)y_\pm} = \mathrm{SNR}, \tag{4.48}$$

which implies that the spatial frequency will be cut off for those below the noise level and the surface deformation parameter.

Taking into account the frequency cut-off, we have regularized reconstruction formulas

$$\hat{f}_{\varepsilon,\delta}(\xi) = C^{-1}(\xi,\kappa_\pm)\left(\hat{w}^\delta(\xi,y_\pm) - \hat{w}_0^\pm(\xi,y_\pm)\right) e^{\mp i\eta_\pm y_\pm}\, \chi_{[-\omega_\pm,\,\omega_\pm]}(\xi), \tag{4.49}$$

where the characteristic function

$$\chi_{[-\omega_\pm,\omega_\pm]}(\xi) = \begin{cases} 1 & \text{for} \quad |\xi| \le \omega_\pm, \\ 0 & \text{for} \quad |\xi| > \omega_\pm. \end{cases}$$

Define

$$\tilde{f}_0^\pm(\xi) = C^{-1}(\xi,\kappa_\pm)\hat{w}_0^\pm(\xi,y_\pm)e^{\mp i\eta_\pm y_\pm}\,\chi_{[-\omega_\pm,\omega_\pm]}(\xi) \tag{4.50}$$

and

$$\tilde{f}_1^\pm(\xi) = C^{-1}(\xi,\kappa_\pm)\hat{w}^\delta(\xi,y_\pm)e^{\mp i\eta_\pm y_\pm}\,\chi_{[-\omega_\pm,\omega_\pm]}(\xi). \tag{4.51}$$

It follows from the regularized inversion formulation (4.49) that we obtain the reconstructed scattering surface after taking the inverse Fourier transform:

$$\tilde{f}^\pm(x) = (2\pi)^{-1/2}\int_{\mathbb{R}}[\tilde{f}_1^\pm(\xi) - \tilde{f}_0^\pm(\xi)]e^{i\xi x}d\xi. \tag{4.52}$$

Clearly, the reconstructed scattering surface function $\tilde{f}^\pm$ depends on the cut-off frequencies $\omega_\pm$, which depend on the scattering surface deformation parameter ε and the data noise level parameter δ.

For the normal incidence, the leading terms $w_0^\pm$ in (4.11) and (4.12) become

$$w_0^+(x,y) = e^{-i\kappa_+ y} + \left(\frac{\kappa_+ - \kappa_-}{\kappa_+ + \kappa_-}\right)e^{i\kappa_+ y} \quad \text{and} \quad w_0^-(x,y) = \left(\frac{2\kappa_+}{\kappa_+ + \kappa_-}\right)e^{-i\kappa_- y},$$

where the reflection coefficient r and the transmission coefficient t are defined in (4.24). Taking the Fourier transform of $w^\pm(x,y)$ with respect to x yields

$$\hat{w}_0^+(\xi,y) = (2\pi)^{1/2}\left[e^{-i\kappa_+ y} + \left(\frac{\kappa_+ - \kappa_-}{\kappa_+ + \kappa_-}\right)e^{i\kappa_+ y}\right]\delta(\xi)$$

and

$$\hat{w}_0^-(\xi,y) = (2\pi)^{1/2}\left[\left(\frac{2\kappa_+}{\kappa_+ + \kappa_-}\right)e^{-i\kappa_- y}\right]\delta(\xi).$$

It may be verified from (4.30) and (4.44) that

$$C(0,\kappa_\pm) = C_0(0,\kappa_\pm) + \frac{2i\kappa_+\kappa_-}{\kappa_+ + \kappa_-} = -\frac{2i\kappa_+(\kappa_+ - \kappa_-)}{\kappa_+ + \kappa_-}.$$

Noting (4.36), (4.42), and (4.50), we obtain

$$\begin{aligned}(2\pi)^{-1/2}\int_{\mathbb{R}}\tilde{f}_0^+(\xi)e^{i\xi x}d\xi &= C^{-1}(0,\kappa_\pm)\left[e^{-i\kappa_+ y_+} + \left(\frac{\kappa_+ - \kappa_-}{\kappa_+ + \kappa_-}\right)e^{i\kappa_+ y_+}\right]e^{-i\kappa_+ y_+} \\ &= \frac{i}{2\kappa_+}\left[\left(\frac{\kappa_+ + \kappa_-}{\kappa_+ - \kappa_-}\right)e^{-2i\kappa_+ y_+} + 1\right]\end{aligned}$$

and

$$(2\pi)^{-1/2}\int_{\mathbb{R}}\tilde{f}_0^-(\xi)e^{\mathrm{i}\xi x}d\xi = C^{-1}(0,\kappa_\pm)\left[\left(\frac{2\kappa_+}{\kappa_+ + \kappa_-}\right)e^{-\mathrm{i}\kappa_- y_-}\right]e^{\mathrm{i}\kappa_- y_-} = \mathrm{i}(\kappa_+ - \kappa_-)^{-1}.$$

Therefore, the regularized inversion formulas (4.49) can be finally written as

$$\tilde{f}(x) = (2\pi)^{-1/2}\int_{\mathbb{R}}\tilde{f}_1^+(\xi)e^{\mathrm{i}\xi x}d\xi - \frac{\mathrm{i}}{2\kappa_+}\left[\left(\frac{\kappa_+ + \kappa_-}{\kappa_+ - \kappa_-}\right)e^{-2\mathrm{i}\kappa_+ y_+} + 1\right] \tag{4.53}$$

and

$$\tilde{f}(x) = (2\pi)^{-1/2}\int_{\mathbb{R}}\tilde{f}_1^-(\xi)e^{\mathrm{i}\xi x}d\xi - \mathrm{i}(\kappa_+ - \kappa_-)^{-1}. \tag{4.54}$$

As shown in (4.53) and (4.54), one Fourier transform and one inverse Fourier transform are needed to reconstruct the scattering surface function for either the reflection configuration or the transmission configuration. These transforms are realized by the FFT in our numerical experiments.

5. Numerical experiments. In this section, we discuss the implementation for the direct and inverse surface scattering problems, present three numerical examples to illustrate the effectiveness of the proposed method, and examine the dependence of resolution on all three parameters: measurement distance $|y_\pm|$, surface deformation parameter ε, and the noise level δ. Three types of surfaces are considered: a locally perturbed smooth surface, an oscillatory periodic smooth surface, and a nonsmooth piecewise constant surface.

In practice, the open domain needs to be truncated into a bounded domain in order to solve the direct problem and obtain the synthetic scattering data. Suitable boundary conditions have to be imposed on the boundary of the bounded domain so that no artificial wave reflection occurs to ruin the wave field inside the domain. In section 2, a transparent boundary condition is introduced in the y-direction. However, this nonreflecting boundary condition is nonlocal and involves the issue of the Fourier transform in the whole $\mathbb{R}$. In addition, an appropriate boundary condition needs to be considered in the x-direction. Since the focus is on the inverse problem in this work, we consider special examples: the scattering surfaces are even functions. Due to the symmetry of the problem, normal incidence, and even scattering surfaces, the solutions to the direct problem are also symmetric to the y-axis and thus the periodic boundary condition can be used in the x-direction. In the y-direction, we adopt a convenient perfectly matched layer (PML) technique to truncate the open domain [19]. The scattering data is obtained by the numerical solution of the direct scattering problem, which is implemented by using the finite element method.

In the following three examples, the incident wave is taken as a single plane wave with normal incidence, i.e., $u^{\mathrm{inc}}(x,y) = e^{-\mathrm{i}\kappa_+ y}$. The wavenumber above the scattering surface is $\kappa_+ = 2\pi$, which corresponds to the wavelength $\lambda = 1$, and the wavenumber below the scattering surface is $\kappa_- = 2\pi(4.0+\mathrm{i})^{1/2}$, which is exemplary and stands for a general substrate with a complex permittivity. Since the results are similar for the reflection configuration and the transmission configuration, we shall present only the examples for the reflection configuration and use h to stand for the measurement distance y_+, i.e., $h = y_+$. In all the

figures, the plots were rescaled with respect to the wavelength λ. The computational domain for the direct problem is $[-0.5,\ 0.5] \times [-0.5,\ 0.5]$ with the PML region $[-0.5,\ 0.5] \times [-0.5, -0.3] \cup [-0.5,\ 0.5] \times [0.3,\ 0.5]$. Due to the unstructured triangular meshes, the wave field data $u(x, h)$ is not equally spaced with respect to x. We construct a curve $u(x, h)$ by using the natural cubic spline interpolation formula based on the computed discrete data $u(x, h)$. The curve $u(x, h)$ is evaluated at equally spaced points $x_j, j = 0, 1, \ldots, 512$, in the interval $[-0.5, 0.5]$ and used as our synthetic scattering data.

To test the stability of the method, some relative random noise is added to the scattering data; i.e., the scattering data takes the form

$$u^\delta(x, h) = u(x, h)(1 + \delta\,\mathrm{rand}),$$

where rand stands for uniformly distributed random numbers in $[-1,\ 1]$.

Example 1. This example illustrates the results for a locally perturbed smooth surface. The exact scattering surface is given by $f(x) = \varepsilon g(x)$, where

$$g(x) = \cos(6\pi x)e^{-20x^2}.$$

We examine the effects of y_+, δ, and ε on the reconstructions.

First consider the measurement distance h. The surface deformation parameter was fixed as $\varepsilon = 0.01$. Besides the error from the linearization by dropping higher order terms in the power series, a small amount of noise with $\delta = 0.1\%$ is added to the data. Figure 2 shows the reconstructed surfaces (dashed curves) against the exact surfaces (solid curves) by using the scattering data measured at different distances $h = 0.1\lambda$, 0.15λ, 0.2λ, and 0.25λ. It is clear that a smaller measurement distance gives better reconstruction results. The fine features of the scattering surface are completely recovered, and the subwavelength resolution is obviously achieved especially when using $h = 0.1\lambda$. This is attributed to the fact that the larger cut-off frequency ω_+ may be used in the inversion formula when the measurement distance h is smaller for fixed SNR, i.e., fixed ε and δ.

Next consider the noise level parameter δ. The surface deformation parameter and the measurement distance were fixed as $\varepsilon = 0.01$ and $h = 0.02\lambda$, respectively. Figure 3 plots the reconstructed surfaces (dashed curves) against the exact surfaces (solid curves) by using the scattering data with different noise levels $\delta = 0.01$, 0.02, 0.03, 0.04. It can be seen that smaller noise levels yield better reconstruction results. As expected from the relation between the cut-off frequency and the SNR in (4.48), a larger noise level parameter δ means a smaller SNR and thus a smaller cut-off frequency ω in order to get a stable reconstruction.

Finally consider the surface deformation parameter ε. The measurement distance $h = 0.08\lambda$, and $\delta = 0.1\%$ noise is added to the data. Figure 4 shows the reconstructed surfaces (dashed curves) against the exact surfaces (solid curve) by using the scattering data with different surface deformation parameters $\varepsilon = 0.01$, 0.02, 0.03, 0.04. Clearly, smaller ε gives better reconstruction. All the fine features are recovered especially when using $\varepsilon = 0.01$. Although some amplitude information is not completely correct, all the phase information is still correctly reconstructed even for large ε. It can be seen from the power series (4.2) that the linearization procedure (4.5) gives more accurate approximation to the original nonlinear inverse problem if the surface deformation parameter ε is smaller. For fixed ε and h, smaller

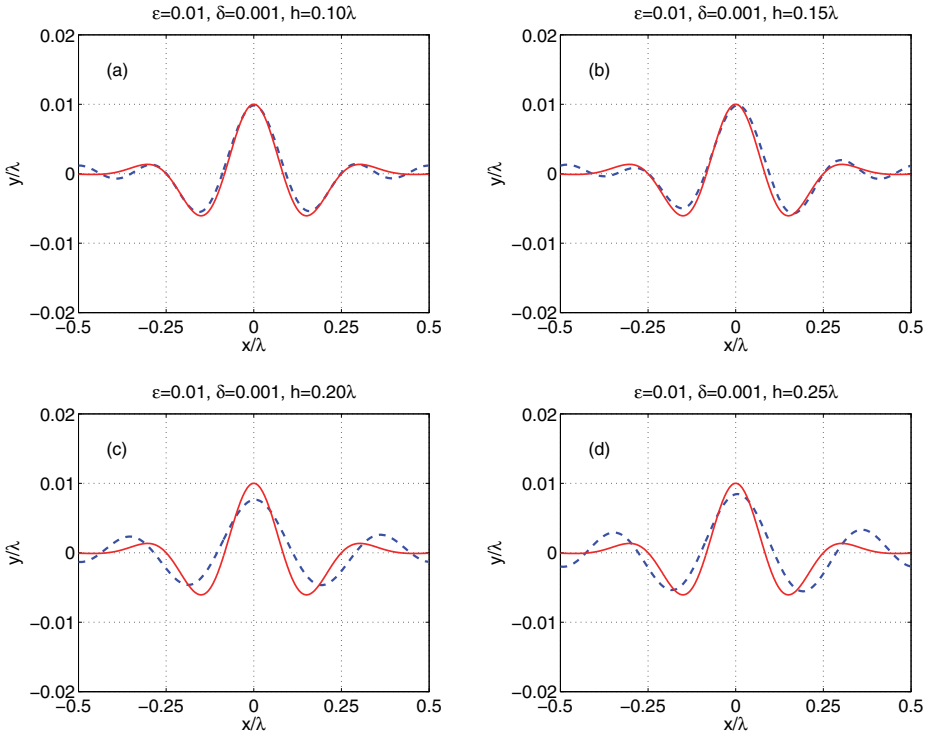

Figure 2. *Example* 1: *A locally perturbed smooth surface. Exact surfaces (solid curves) are plotted against reconstructed surfaces (dashed curves) using the scattering data measured at different heights of* h. (a) $h = 0.10\lambda$; (b) $h = 0.15\lambda$; (c)$h = 0.20\lambda$; (d) $h = 0.25\lambda$.

δ means larger SNR and thus larger cut-off frequency ω, which contributes to a better and sharper reconstruction.

Based on the above observation, it can be concluded that a smaller measurement distance (as small as possible) is preferred in order to obtain a stable reconstruction with a superresolved resolution, which confirms the principle of near-field optical imaging.

Example 2. This example uses an oscillatory periodic smooth surface to illustrate the results for a nonlocally perturbed plane surface. The exact scattering surface is described by the periodic function $f(x) = \varepsilon g(x)$ with

$$g(x) = \cos(2\pi x) - 0.2\cos(20\pi x).$$

For this example, we will not show the investigation of the reconstructions on all the parameters since the results and conclusions are the same as those for the first example. This scattering surface is much more oscillatory and has finer features than the first example does. It is expected to use larger cut-off frequency ω in order to completely resolve all the features and get a superresolved resolution for the construction, which requires smaller measurement distance h. Figure 5 shows the reconstructed surfaces (dashed curves) against the exact surfaces (solid curves) by using the scattering data with four different sets of parameters of (ε, δ, h): $(\varepsilon = 0.01, \delta = 0.001, h = 0.02\lambda)$; $(\varepsilon = 0.01, \delta = 0.001, h = 0.05\lambda)$; $(\varepsilon = 0.01, \delta = 0.01, h = 0.02\lambda)$; $(\varepsilon = 0.02, \delta = 0.01, h = 0.02\lambda)$. Again, it can be seen that a smaller surface

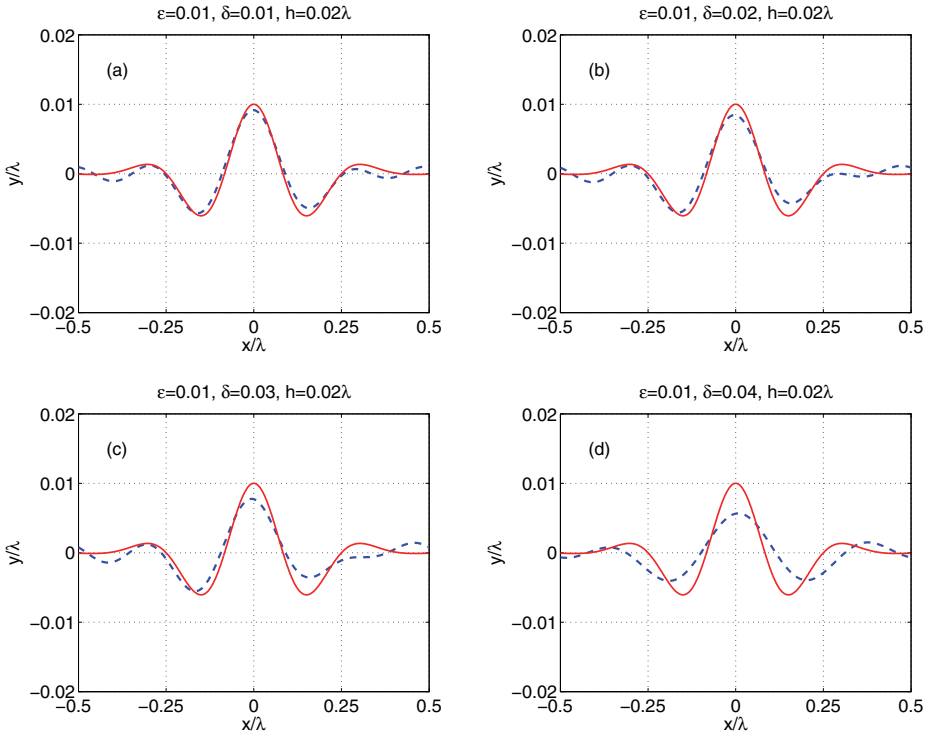

Figure 3. *Example* 1: *A locally perturbed smooth surface. Exact surfaces (solid curves) are plotted against reconstructed surfaces (dashed lines) using the scattering data with different noise levels of* δ. (a) $\delta = 0.01$; (b) $\delta = 0.02$; (c) $\delta = 0.03$; (d) $\delta = 0.04$.

deformation parameter h is needed in order to achieve equally good reconstruction for a larger noise level parameter δ.

Example 3. This example uses a piecewise constant scattering surface to illustrate that the method can also be applied to nonsmooth functions, though the mathematical justification is shown only for smooth surfaces. The exact scattering surface is described by the periodic function $f(x) = \varepsilon g(x)$, where

$$g(x) = \begin{cases} 1 & \text{in} \quad (-0.3, \ -0.1) \cup (0.1, \ 0.3), \\ 0 & \text{in} \quad [-0.5, \ -0.3] \cup [-0.1, \ 0.1] \cup [0.3, \ 0.5]. \end{cases}$$

Again, we will not show the investigation of the reconstructions on all the parameters since the results and conclusions are the same as those for the first example. In this example, the function is discontinuous. It is well known that the piecewise constant function contains infinitely many Fourier coefficients that decay slowly, and the oscillatory behavior near the discontinuities displays the well-known Gibbs phenomenon. Figure 6 shows the reconstructed surfaces (dashed curves) against the exact surfaces (solid lines) by using the scattering data with four different sets of parameters of (ε, δ, h): $(\varepsilon = 0.01, \delta = 0.001, h = 0.02\lambda)$; $(\varepsilon = 0.01, \delta = 0.001, h = 0.05\lambda)$; $(\varepsilon = 0.01, \delta = 0.01, h = 0.02\lambda)$; $(\varepsilon = 0.02, \delta = 0.01, h = 0.02\lambda)$.

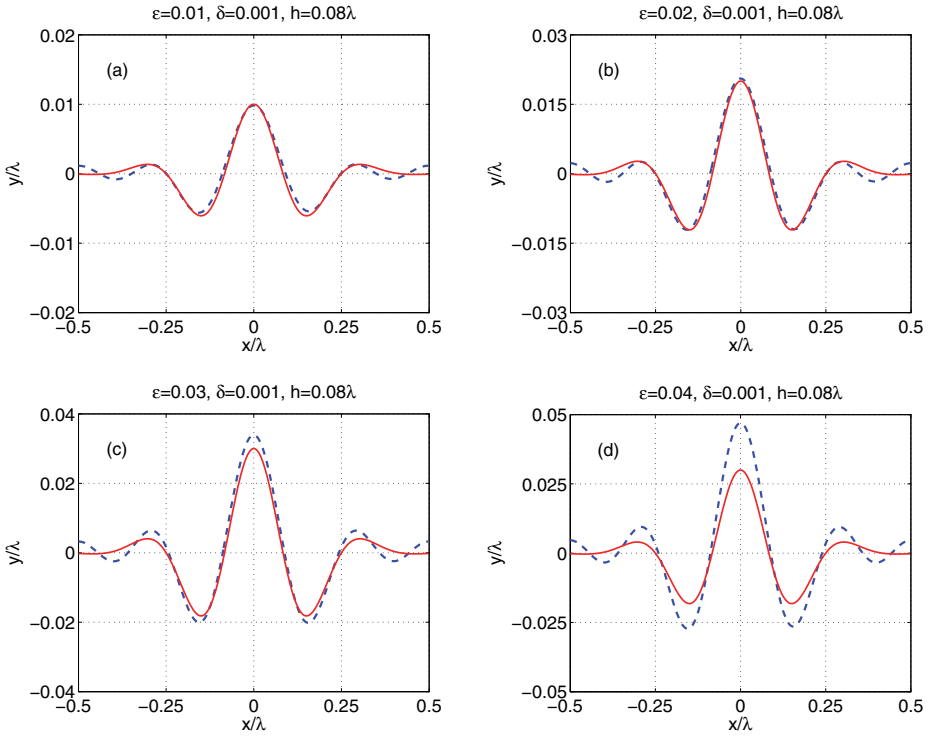

Figure 4. *Example* 1: *A locally perturbed smooth surface. Exact surfaces (solid curves) are plotted against reconstructed surfaces (dashed curves) with different surface deformation parameters of* ε. (a) $\varepsilon = 0.01$; (b) $\varepsilon = 0.02$; (c) $\varepsilon = 0.03$; (d) $\varepsilon = 0.04$.

Similarly, it can be seen that a smaller surface deformation parameter h is needed in order to achieve equally good reconstruction for a larger noise level parameter δ.

6. Concluding remarks. We have presented a simple, stable, and effective method for solving an inverse surface scattering problem in near-field optical imaging of dielectric media, where the wave is allowed to penetrate the substrate below the scattering surface. The scattering surface model is assumed to be a small and smooth deformation of a plane surface. Using transformed field expansion, the scattering problem with a complex scattering surface may be converted into a successive sequence of a two-point boundary value problem in the frequency domain. An analytical solution for the direct scattering problem is deduced from the method of integration solution. By dropping the high order terms in the asymptotic expansion, the nonlinear inverse problem is linearized to obtain explicit and unified inversion formulas for both the reflection configuration and the transmission configuration. The cut-off frequency is chosen from the SNR analysis which depends on the surface deformation parameter, noise level, and the measurement distance. The reconstruction method requires only a single illumination at a fixed frequency and is implemented efficiently by executing two FFTs, one for the data processing and another for the inversion. Three types of scattering surfaces are considered, a locally perturbed surface, an oscillatory periodic surface, and a nonsmooth surface. The effects of the deformation parameter, noise level, and measurement distance

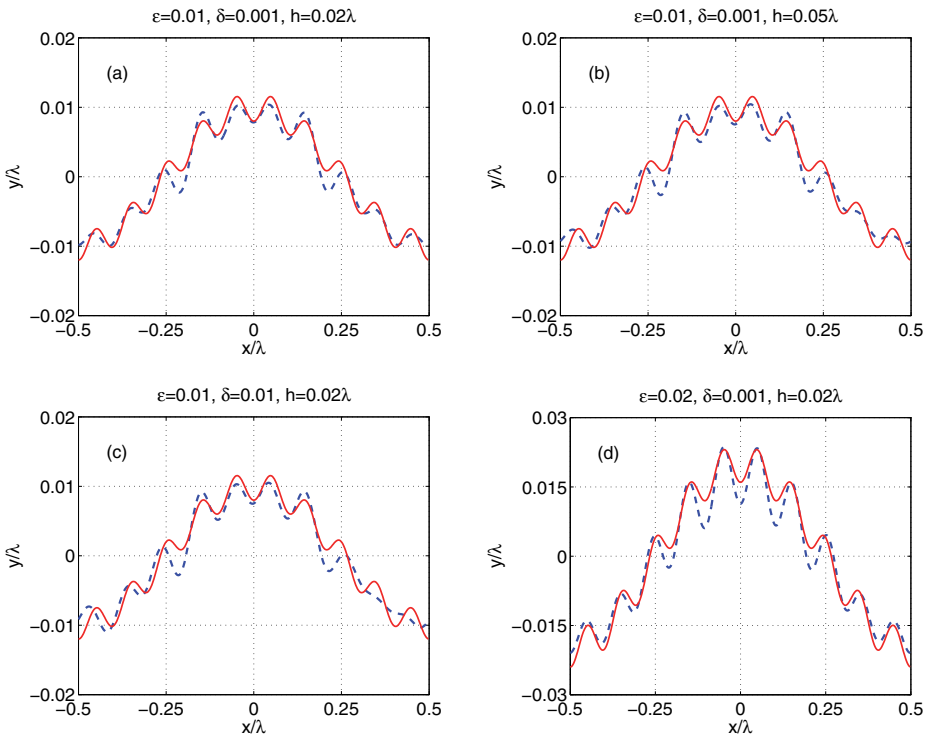

Figure 5. *Example 2: An oscillatory periodic smooth scattering surface. Exact surfaces (solid curves) are plotted against reconstructed surfaces (dashed curves) with four different sets of parameters of ε, δ, and y_+: (a) $\varepsilon = 0.01, \delta = 0.001, y_+ = 0.02\lambda$; (b) $\varepsilon = 0.01, \delta = 0.001, y_+ = 0.05\lambda$; (c) $\varepsilon = 0.01, \delta = 0.01, y_+ = 0.02\lambda$; (d) $\varepsilon = 0.02, \delta = 0.001, y_+ = 0.02\lambda$.*

were reported on the resolution of the reconstruction. The results show that superresolved resolution may be achieved for small measurement distance, which confirms the principle of near-field optical imaging.

We point out some future directions along the line of inverse surface scattering in near-field imaging. In this paper, the scattering surface is assumed to be a small deformation of a plane surface, and the linearized inverse problem is a good approximation of the original nonlinear inverse problem. Results show that the accuracy of the reconstruction deteriorates as the deformation parameter is increased. Thus the linear mode may not be sufficient and the nonlinear model needs to be considered for scattering surfaces with large deviation. It is interesting and challenging to solve the inverse surface scattering using phaseless data and the model of Maxwell's equations for electromagnetic wave propagation. An even more challenging problem is to consider a random surface scattering problem where the scattering surface is modeled by a random function instead of a deterministic function. We hope to be able to address these issues and report the progress elsewhere in the future.

Appendix A. Integration solution method. In this section, the integrated solution method is briefly introduced to solve a two-point boundary value problem. We refer the reader to Zhang [44] for the details of the integrated solutions of ordinary differential equation systems and two-point boundary value problems.

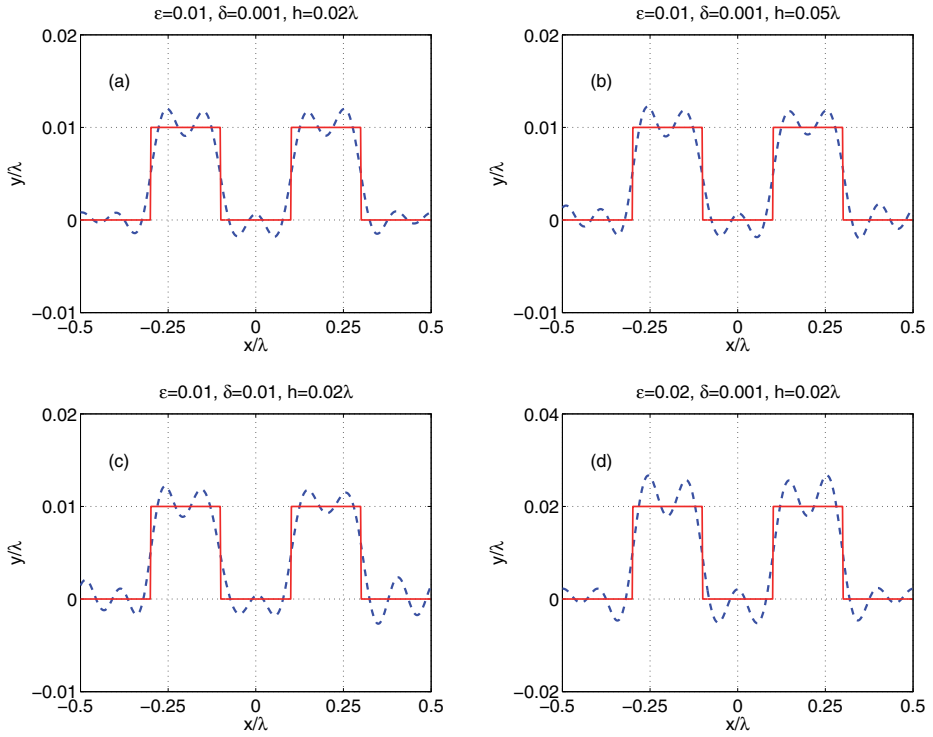

Figure 6. *Example* 3: *A nonsmooth piecewise constant scattering surface. Exact surfaces (solid lines) are plotted against reconstructed surfaces (dashed curves) with four different sets of parameters* ε, δ, *and* h: (a) $\varepsilon = 0.01, \delta = 0.001, h = 0.02\lambda$; (b) $\varepsilon = 0.01, \delta = 0.001, h = 0.05\lambda$; (c) $\varepsilon = 0.01, \delta = 0.01, h = 0.02\lambda$; (d) $\varepsilon = 0.02, \delta = 0.001, h = 0.02\lambda$.

Consider the two-point boundary value problem

$$\mathbf{u}'(y) + M(y)\mathbf{u}(y) = \mathbf{f}(y), \tag{A.1}$$

$$A_0\mathbf{u}(y)|_{y=0} = \mathbf{r}_0, \tag{A.2}$$

$$B_1\mathbf{u}(y)|_{y=b} = \mathbf{s}_1, \tag{A.3}$$

where $\mathbf{f}(y) \in \mathbb{C}^m$ are m-dimensional vector fields, $\mathbf{r}_0 \in \mathbb{C}^{m_1}$ and $\mathbf{s}_1 \in \mathbb{C}^{m_2}$ are given m_1- and m_2-dimensional vector fields, respectively, $M(y) \in \mathbb{C}^{m\times m}$ is an $m \times m$ matrix, and $A_0 \in \mathbb{C}^{m_1\times m}$ and $B_1 \in \mathbb{C}^{m_2\times m}$ are full rank matrices with $m_1 + m_2 = m$, i.e., $\mathrm{rank}A_0 = m_1$ and $\mathrm{rank}B_1 = m_2$.

Let $\Phi(y)$ be the fundamental matrix of the system

$$\Phi'(y) + M(y)\Phi(y) = \mathbf{0}, \tag{A.4}$$

$$\Phi(0) = I_m, \tag{A.5}$$

where I_m is the $m \times m$ identity matrix.

Theorem A.1. *The two-point boundary value problem* (A.1)–(A.3) *has a unique solution if and only if*

$$\det \begin{bmatrix} A_0 \\ B_1\Phi(b) \end{bmatrix} \neq 0. \tag{A.6}$$

Let the pair of functions $\{A(y), \mathbf{r}(y)\}$ and $\{B(y), \mathbf{s}(y)\}$ be the integrated solutions of the problems (A.1)–(A.2) and (A.1)–(A.3), respectively; then there exist $D_0(A, y) \in \mathbb{C}^{m_1\times m_1}$ and $D_1(B, y) \in \mathbb{C}^{m_2\times m_2}$ such that

$$A' = AM + D_0A, \quad A(0) = A_0, \tag{A.7}$$

$$\mathbf{r}' = A\mathbf{f} + D_0\mathbf{r}, \quad \mathbf{r}(0) = \mathbf{r}_0, \tag{A.8}$$

and

$$B' = BM + D_1B, \quad B(b) = B_1, \tag{A.9}$$

$$\mathbf{s}' = B\mathbf{f} + D_1\mathbf{s}, \quad \mathbf{s}(b) = \mathbf{s}_1. \tag{A.10}$$

Theorem A.2. *If the two-point boundary value problem* (A.1)–(A.3) *has a unique solution, then the matrix*

$$\begin{bmatrix} A(y) \\ B(y) \end{bmatrix} \in \mathbb{C}^{m\times m}$$

is nonsingular.

Theorem A.3. *The two-point boundary value problem* (A.1)–(A.3) *is equivalent to the linear system*

$$\begin{bmatrix} A(y) \\ B(y) \end{bmatrix} \mathbf{u}(y) = \begin{bmatrix} \mathbf{r}(y) \\ \mathbf{s}(y) \end{bmatrix}. \tag{A.11}$$

Appendix B. Two-point boundary value problems. In this section, we discuss an application of the integration method for solving two specific two-point boundary value problems, whose solution will be useful for solving the direct surface scattering problem.

Consider a two-point boundary value problem

$$u'' + \eta^2 u = f, \quad 0 < y < b, \tag{B.1}$$

$$u = g \quad \text{at } y = 0, \tag{B.2}$$

$$u' - \mathrm{i}\eta u = h \quad \text{at } y = b. \tag{B.3}$$

Let $v_1 = u$ and $v_2 = u'$. The second order boundary value problem (B.1)–(B.3) can be equivalently formulated into a first order two-point boundary value problem:

$$\mathbf{v}' + M\mathbf{v} = \mathbf{f}, \tag{B.4}$$

$$A_0\mathbf{v}(0) = g, \tag{B.5}$$

$$B_1\mathbf{v}(b) = h, \tag{B.6}$$

where

$$\mathbf{v} = \begin{bmatrix} v_1 \\ v_2 \end{bmatrix}, \quad \mathbf{f} = \begin{bmatrix} 0 \\ f \end{bmatrix}, \quad M = \begin{bmatrix} 0 & -1 \\ \eta^2 & 0 \end{bmatrix},$$

and

$$A_0 = [1 \quad 0], \quad B_1 = [-\mathrm{i}\eta \quad 1].$$

Theorem B.1. *The boundary value problem* (B.1)–(B.3) *has a unique solution, given by*

$$u(y) = e^{\mathrm{i}\eta y} g + K_1(y) h - \int_0^b K_2(y,z) f(z) dz, \tag{B.7}$$

where

$$K_1(y) = \frac{e^{\mathrm{i}\eta b}}{2\mathrm{i}\eta} \left(e^{\mathrm{i}\eta y} - e^{-\mathrm{i}\eta y}\right), \quad K_2(y,z) = \begin{cases} \dfrac{e^{\mathrm{i}\eta y}}{2\mathrm{i}\eta} \left(e^{\mathrm{i}\eta z} - e^{-\mathrm{i}\eta z}\right), & z < y, \\ \dfrac{e^{\mathrm{i}\eta z}}{2\mathrm{i}\eta} \left(e^{\mathrm{i}\eta y} - e^{-\mathrm{i}\eta y}\right), & z > y. \end{cases}$$

Proof. Since M is a nonsingular matrix, there exists a nonsingular matrix Q such that

$$Q^{-1} M Q = N,$$

where

$$N = \begin{bmatrix} -\mathrm{i}\eta & 0 \\ 0 & \mathrm{i}\eta \end{bmatrix}, \quad Q = \begin{bmatrix} 1 & 1 \\ \mathrm{i}\eta & -\mathrm{i}\eta \end{bmatrix}, \quad \text{and} \quad Q^{-1} = \frac{1}{2\mathrm{i}\eta} \begin{bmatrix} \mathrm{i}\eta & 1 \\ \mathrm{i}\eta & -1 \end{bmatrix}.$$

A simple calculation yields that the fundamental matrix of (A.4)–(A.5) is

$$\Phi(y) = Q \begin{bmatrix} e^{\mathrm{i}\eta y} & \\ & e^{-\mathrm{i}\eta y} \end{bmatrix} Q^{-1},$$

which gives

$$\det \begin{bmatrix} A_0 \\ B_1 \Phi(b) \end{bmatrix} = \begin{vmatrix} 1 & 0 \\ -\mathrm{i}\eta e^{-\mathrm{i}\eta b} & e^{-\mathrm{i}\eta b} \end{vmatrix} = e^{-\mathrm{i}\eta b} \neq 0.$$

It follows from Theorem A.1 that the two-point boundary value problem (B.4)–(B.6) and thus (B.1)–(B.3) have a unique solution.

Let $\{A(y), r(y)\}$ and $\{B(y), s(y)\}$ be the integrated solutions of the problems (B.4), (B.5) and (B.4), (B.6), respectively. Taking

$$D_0 = \mathrm{i}\eta, \quad D_1 = -\mathrm{i}\eta,$$

we obtain from (A.7)–(A.10) that the integrated solutions satisfy

$$A' = AM + \mathrm{i}\eta A, \quad A(0) = A_0, \tag{B.8}$$

$$r' = A\mathbf{f} + \mathrm{i}\eta r, \quad r(0) = g, \tag{B.9}$$

and

$$B' = BM - \mathrm{i}\eta B, \quad B(h) = B_1, \tag{B.10}$$

$$s' = B\mathbf{f} - \mathrm{i}\eta s, \quad s(b) = h. \tag{B.11}$$

Upon solving the above initial value problem, we obtain the integrated solutions

$$A = [A_1 \ A_2] = \frac{1}{2\mathrm{i}\eta}\left[\mathrm{i}\eta(1 + e^{2\mathrm{i}\eta y}) \quad 1 - e^{2\mathrm{i}\eta y}\right], \tag{B.12}$$

$$B = [B_1 \ B_2] = [-\mathrm{i}\eta \quad 1], \tag{B.13}$$

$$r = e^{\mathrm{i}\eta y} g + \int_0^y e^{\mathrm{i}\eta(y-z)} A_2(z) f(z) dz, \tag{B.14}$$

$$s = e^{\mathrm{i}\eta(b-y)} h - \int_y^b e^{\mathrm{i}\eta(z-y)} f(z) dz. \tag{B.15}$$

It follows from Theorem A.3 that the two-point boundary value problem (B.4)–(B.6) is equivalent to the linear system

$$\begin{bmatrix} A_1 & A_2 \\ B_1 & B_2 \end{bmatrix} \begin{bmatrix} u \\ u' \end{bmatrix} = \begin{bmatrix} r \\ s \end{bmatrix}.$$

An application of Gram's rule yields

$$u = \frac{rB_2 - sA_2}{A_1 B_2 - B_1 A_2}. \tag{B.16}$$

A simple calculation yields

$$A_1 B_2 - B_1 A_2 = 1.$$

Substituting (B.12)–(B.15) into (B.16), we deduce (B.7). ∎

Consider another two-point boundary value problem

$$u'' + \eta^2 u = f, \quad a < y < 0, \tag{B.17}$$

$$u = g \quad \text{at } y = 0, \tag{B.18}$$

$$u' + \mathrm{i}\eta u = h \quad \text{at } y = a. \tag{B.19}$$

Let $v_1 = u$ and $v_2 = u'$. The second order boundary value problem (B.17)–(B.19) can be equivalently formulated into a first order two-point boundary value problem:

$$\mathbf{v}' + M\mathbf{v} = \mathbf{f}, \tag{B.20}$$

$$A_0 \mathbf{v}(0) = g, \tag{B.21}$$

$$B_1 \mathbf{v}(a) = h, \tag{B.22}$$

where

$$\mathbf{v} = \begin{bmatrix} v_1 \\ v_2 \end{bmatrix}, \quad \mathbf{f} = \begin{bmatrix} 0 \\ f \end{bmatrix}, \quad M = \begin{bmatrix} 0 & -1 \\ \eta^2 & 0 \end{bmatrix},$$

and

$$A_0 = [1 \quad 0], \quad B_1 = [\mathrm{i}\eta \quad 1].$$

We may follow the same steps to show that the boundary value problem (B.17)–(B.19) and the two-point boundary value problem (B.20)–(B.22) have a unique solution. The details are skipped here for simplicity.

Theorem B.2. *The boundary value problem* (B.17)–(B.19) *has a unique solution, given by*

$$u(y) = e^{-\mathrm{i}\eta y} g + K_1(y)h + \int_a^0 K_2(y,z) f(z) dz, \tag{B.23}$$

where

$$K_1(y) = \frac{e^{-\mathrm{i}\eta a}}{2\mathrm{i}\eta}\left(e^{\mathrm{i}\eta y} - e^{-\mathrm{i}\eta y}\right), \quad K_2(y,z) = \begin{cases} \dfrac{e^{-\mathrm{i}\eta z}}{2\mathrm{i}\eta}\left(e^{\mathrm{i}\eta y} - e^{-\mathrm{i}\eta y}\right), & z < y, \\ \dfrac{e^{-\mathrm{i}\eta y}}{2\mathrm{i}\eta}\left(e^{\mathrm{i}\eta z} - e^{-\mathrm{i}\eta z}\right), & z > y. \end{cases}$$

REFERENCES

[1] I. Akduman, R. Kress, and A. Yapar, *Iterative reconstruction of dielectric rough surface profiles at fixed frequency*, Inverse Problems, 22 (2006), pp. 939–954.

[2] H. Ammari and T. Abbound, *Diffraction at a curved grating: TM and TE cases, homogenization*, J. Math. Anal. Appl., 202 (1996), pp. 995–1026.

[3] H. Ammari, G. Bao, and A. Wood, *An integral equation method for the electromagnetic scattering from cavities*, Math. Methods Appl. Sci., 23 (2000), pp. 1057–1072.

[4] H. Ammari, J. Garnier, and K. Sølna, *Resolution and stability analysis in full-aperture, linearized conductivity and wave imaging*, Proc. Amer. Math. Soc., 141 (2013), pp. 3431–3446.

[5] H. Ammari, J. Garnier, and K. Sølna, *Partial data resolving power of conductivity imaging from boundary measurements*, SIAM J. Math. Anal., 45 (2013), pp. 1704–1722.

[6] G. Bao, L. Cowsar, and W. Masters, eds., *Mathematical Modeling in Optical Science*, Frontiers Appl. Math. 22, SIAM, Philadelphia, 2001.

[7] G. Bao, D. Dobson, and J. A. Cox, *Mathematical studies in the rigorous grating theory*, J. Opt. Soc. Amer. A, 12 (1995), pp. 1029–1042.

[8] G. Bao, J. Gao, and P. Li, *Analysis of direct and inverse cavity scattering problems*, Numer. Math. Theory Methods Appl., 4 (2011), pp. 335–358.

[9] G. Bao and P. Li, *Near-field imaging of infinite rough surfaces*, SIAM J. Appl. Math., 73 (2013), pp. 2162–2187.

[10] G. Bao, P. Li, and J. Lv, *Numerical solution of an inverse diffraction grating problem from phaseless data*, J. Opt. Soc. Amer. A, 30 (2013), pp. 293–299.

[11] G. Bao, P. Li, and H. Wu, *A computational inverse diffraction grating problem*, J. Opt. Soc. Amer. A, 29 (2012), pp. 394–399.

[12] G. Bao and J. Lin, *Near-field imaging of the surface displacement on an infinite ground plane*, Inverse Probl. Imaging, 7 (2013), pp. 377–396.

[13] O. Bruno and F. Reitich, *Numerical solution of diffraction problems: A method of variation of boundaries*, J. Opt. Soc. Amer. A, 10 (1993), pp. 1168–1175.

[14] P. S. Carney and J. C. Schotland, *Inverse scattering for near-field microscopy*, Appl. Phys. Lett., 77 (2000), pp. 2798–2800.

[15] P. S. Carney and J. C. Schotland, *Near-field tomography*, in Inside Out: Inverse Problems and Applications, Math. Sci. Res. Inst. Publ. 47, Cambridge University Press, Cambridge, UK, 2003, pp. 133–168.

[16] S. N. Chandler-Wilde and P. Monk, *Existence, uniqueness, and variational methods for scattering by unbounded rough surfaces*, SIAM J. Math. Anal., 37 (2005), pp. 598–618.
[17] S. N. Chandler-Wilde and B. Zhang, *A uniqueness result for scattering by infinite rough surfaces*, SIAM J. Appl. Math., 58 (1998), pp. 1774–1790.
[18] S. N. Chandler-Wilde, C. R. Ross, and B. Zhang, *Scattering by infinite one-dimensional rough surfaces*, R. Soc. Lond. Proc. Ser. A Math. Phys. Eng. Sci., 455 (1999), pp. 3767–3787.
[19] Z. Chen and H. Wu, *An adaptive finite element method with perfectly matched absorbing layers for the wave scattering by periodic structures*, SIAM J. Numer. Anal., 41 (2003), pp. 799–826.
[20] R. Coifman, M. Goldberg, T. Hrycak, M. Israeli, and V. Rokhlin, *An improved operator expansion algorithm for direct and inverse scattering computations*, Waves Random Media, 9 (1999), pp. 441–457.
[21] D. Colton and R. Kress, *Inverse Acoustic and Electromagnetic Scattering Theory*, Appl. Math. Sci. 93, Springer-Verlag, Berlin, 1998.
[22] D. Courjon, *Near-Field Microscopy and Near-Field Optics*, Imperial College Press, London, 2003.
[23] D. Courjon and C. Bainier, *Near field microscopy and near field optics*, Rep. Prog. Phys., 57 (1994), pp. 989–1028.
[24] G. Derveaux, G. Papanicolaou, and C. Tsogka, *Resolution and denoising in near-field imaging*, Inverse Problems, 22 (2006), pp. 1437–1456.
[25] J. A. DeSanto and P. A. Martin, *On the derivation of boundary integral equations for scattering by an infinite one-dimensional rough surface*, J. Acoust. Soc. Amer., 102 (1997), pp. 67–77.
[26] J. A. DeSanto and R. J. Wombell, *The reconstruction of shallow rough-surface profiles from scattered field data*, Inverse Problems, 7 (1991), pp. L7–L12.
[27] H. Engl, M. Hanke, and A. Neubauer, *Regularization of Inverse Problems*, Kluwer Academic Publishers, Dordrecht, The Netherlands, 1996.
[28] C. Girard and A. Dereux, *Near-field optics theories*, Rep. Prog. Phys., 59 (1996), pp. 657–699.
[29] J. Jin, *The Finite Element Method in Electromagnetics*, Wiley & Sons, New York, 2002.
[30] R. Kress and T. Tran, *Inverse scattering for a locally perturbed half-plane*, Inverse Problems, 16 (2000), pp. 1541–1559.
[31] P. Li and J. Shen, *Analysis of the scattering by an unbounded rough surface*, Math. Methods Appl. Sci., 35 (2012), pp. 2166–2184.
[32] P. Li and A. Wood, *A two-dimensional Helmholtz equation solution for the multiple cavity scattering problem*, J. Comput. Phys., 240 (2013), pp. 100–120.
[33] P. Li, H. Wu, and W. Zheng, *Electromagnetic scattering by unbounded rough surfaces*, SIAM J. Math. Anal., 43 (2011), pp. 1205–1231.
[34] C. D. Lines and S. N. Chandler-Wilde, *A time domain point source method for inverse scattering by rough surfaces*, Computing, 75 (2005), pp. 157–180.
[35] A. Malcolm and D. P. Nicholls, *A field expansions method for scattering by periodic multilayered media*, J. Acoust. Soc. Amer., 129 (2011), pp. 1783–1793.
[36] A. Malcolm and D. P. Nicholls, *A boundary perturbation method for recovering interface shapes in layered media*, Inverse Problems, 27 (2011), 095009.
[37] D. M. Milder, *An improved formalism for wave scattering from rough surfaces*, J. Acoust. Soc. Amer., 89 (1991), pp. 529–541.
[38] D. P. Nicholls and F. Reitich, *Shape deformations in rough surface scattering: Cancellations, conditioning, and convergence*, J. Opt. Soc. Amer. A, 21 (2004), pp. 590–605.
[39] D. P. Nicholls and F. Reitich, *Shape deformations in rough surface scattering: Improved algorithms*, J. Opt. Soc. Amer. A, 21 (2004), pp. 606–621.
[40] A. G. Voronovich, *Wave Scattering from Rough Surfaces*, Springer, Berlin, 1994.
[41] K. Warnick and W. C. Chew, *Numerical simulation methods for rough surface scattering*, Waves Random Media, 11 (2001), pp. R1–R30.
[42] B. Zhang and S. N. Chandler-Wilde, *Acoustic scattering by an inhomogeneous layer on a rigid plate*, SIAM J. Appl. Math., 58 (1998), pp. 1931–1950.
[43] B. Zhang and S. N. Chandler-Wilde, *Integral equation methods for scattering by infinite rough surfaces*, Math. Methods Appl. Sci., 26 (2003), pp. 463–488.
[44] G.-Q. Zhang, *Integrated solutions of ordinary differential equation system and two-point boundary value problems.* I. *Integrated solution method*, Math. Numer. Sinica, 3 (1981), pp. 245–254.